Article

Cell Reports

Alternative Splicing of P/Q-Type Ca^{2+} Channels Shapes Presynaptic Plasticity

Graphical Abstract

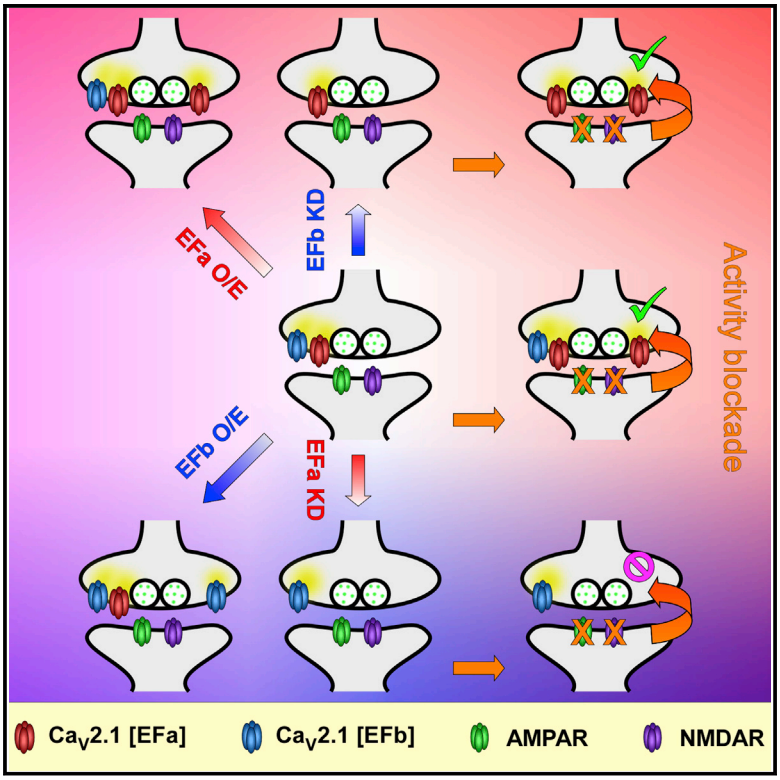

Highlights

- P/Q-type Ca^{2+} channel splice isoforms couple differentially to transmitter release
- The balance between P/Q-type Ca^{2+} channel isoforms contributes to synaptic efficacy
- Splicing of P/Q-type Ca^{2+} channels regulates short-term synaptic plasticity
- Neurons control P/Q-type Ca^{2+} channel isoform levels in a homeostatic fashion

Authors

Agnes Thalhammer, Andrea Contestabile, Yaroslav S. Ermolyuk, ..., Tuck Wah Soong, Yukiko Goda, Lorenzo A. Cingolani

Correspondence

lorenzo.cingolani@iit.it

In Brief

Alternative splicing of Ca^{2+} channels has been hypothesized to contribute to functional diversity in the brain. Thalhammer et al. find that two splice isoforms of P/Q-type Ca^{2+} channels differentially regulate presynaptic plasticity. These results provide evidence that the balance between Ca^{2+} channel isoforms controls synaptic efficacy.

Thalhammer et al., 2017, Cell Reports *20*, 333–343
July 11, 2017
http://dx.doi.org/10.1016/j.celrep.2017.06.055

Cell Reports
Article

Alternative Splicing of P/Q-Type Ca^{2+} Channels Shapes Presynaptic Plasticity

Agnes Thalhammer,[1] Andrea Contestabile,[2] Yaroslav S. Ermolyuk,[3] Teclise Ng,[4,5] Kirill E. Volynski,[3] Tuck Wah Soong,[4,5] Yukiko Goda,[6] and Lorenzo A. Cingolani[1,7,*]

[1]Center for Synaptic Neuroscience and Technology, Istituto Italiano di Tecnologia, Genova 16132, Italy
[2]Department of Neuroscience and Brain Technologies, Istituto Italiano di Tecnologia, Genova 16163, Italy
[3]UCL Institute of Neurology, UCL, London WC1N 3BG, UK
[4]Department of Physiology, Yong Loo Lin School of Medicine, National University of Singapore, Singapore 117456, Singapore
[5]National Neuroscience Institute, 11 Jalan Tan Tock Seng, Singapore 308433, Singapore
[6]RIKEN Brain Science Institute, Wako, Saitama 351-0198, Japan
[7]Lead Contact
*Correspondence: lorenzo.cingolani@iit.it
http://dx.doi.org/10.1016/j.celrep.2017.06.055

SUMMARY

Alternative splicing of pre-mRNAs is prominent in the mammalian brain, where it is thought to expand proteome diversity. For example, alternative splicing of voltage-gated Ca^{2+} channel (VGCC) α_1 subunits can generate thousands of isoforms with differential properties and expression patterns. However, the impact of this molecular diversity on brain function, particularly on synaptic transmission, which crucially depends on VGCCs, is unclear. Here, we investigate how two major splice isoforms of P/Q-type VGCCs ($Ca_v2.1$[EFa/b]) regulate presynaptic plasticity in hippocampal neurons. We find that the efficacy of P/Q-type VGCC isoforms in supporting synaptic transmission is markedly different, with $Ca_v2.1$[EFa] promoting synaptic depression and $Ca_v2.1$[EFb] synaptic facilitation. Following a reduction in network activity, hippocampal neurons upregulate selectively $Ca_v2.1$[EFa], the isoform exhibiting the higher synaptic efficacy, thus effectively supporting presynaptic homeostatic plasticity. Therefore, the balance between VGCC splice variants at the synapse is a key factor in controlling neurotransmitter release and presynaptic plasticity.

INTRODUCTION

The majority of neuronal genes are subject to alternative splicing, which is thought to increase proteome complexity and optimize protein function to specific cellular tasks (Lipscombe et al., 2013; Raj and Blencowe, 2015). In support of a dedicated function of individual splice variants, some mutations that cause brain diseases impair only one of the splice isoforms of a neuronal gene (Simms and Zamponi, 2014) (Figure 1B). Yet there are few studies investigating how alternative splicing regulates physiological events in neurons.

Here, we examine how alternatively spliced variants of $Ca_v2.1$ (P/Q-type) channels, which are the predominant voltage-gated Ca^{2+} channels (VGCCs) at most fast synapses in the CNS, regulate synaptic transmission. Alternative splicing of the pore-forming α_1 subunit of $Ca_v2.1$ (α_{1A}) can potentially generate thousands of splice isoforms displaying differential expression patterns and divergent biophysical properties (Soong et al., 2002). Among them, alternative splicing of the mutually exclusive exons 37a and 37b produces two major variants, $Ca_v2.1$[EFa] and $Ca_v2.1$[EFb], which diverge in an EF-hand-like domain located in the proximal C terminus of the channel (Figures 1A and 1B) (Bourinet et al., 1999; Chaudhuri et al., 2004; Soong et al., 2002). Whereas $Ca_v2.1$[EFb] predominates at early stages of development, both splice isoforms are expressed in comparable amounts in most regions of the adult brain, as for example in the hippocampus (Bourinet et al., 1999; Chaudhuri et al., 2004; Soong et al., 2002; Vigues et al., 2002).

Their biophysical properties, studied in non-neuronal cells to date, differ as well: $Ca_v2.1$[EFa] generates slowly activating currents, whose kinetics are accelerated by Ca^{2+} influx through the channel during a preceding pulse (Ca^{2+}-dependent facilitation), whereas $Ca_v2.1$[EFb] produces currents that are faster than those of $Ca_v2.1$[EFa] under basal conditions and are not further facilitated by Ca^{2+} (Chaudhuri et al., 2004).

Despite prominent expression in the brain and divergent functional properties, it is not known whether these two splice isoforms, or any other $Ca_v2.1$ splice variant, are specialized to fulfill specific cellular tasks in neurons. Here, we have focused on $Ca_v2.1$[EFa] and $Ca_v2.1$[EFb] and asked whether and how they differentially regulate synaptic transmission and plasticity in hippocampal pyramidal neurons.

By manipulating bi-directionally the relative abundance of $Ca_v2.1$[EFa] and $Ca_v2.1$[EFb] isoforms, we reveal that they regulate neurotransmitter release and short-term synaptic plasticity in opposite directions: $Ca_v2.1$[EFa] boosts synaptic efficacy and promotes synaptic depression, while $Ca_v2.1$[EFb] tilts the balance toward low synaptic efficacy and synaptic facilitation. Importantly, neuronal activity regulates the relative abundance of the two $Ca_v2.1$ splice isoforms in a homeostatic fashion. In response to a reduction in network excitability, hippocampal

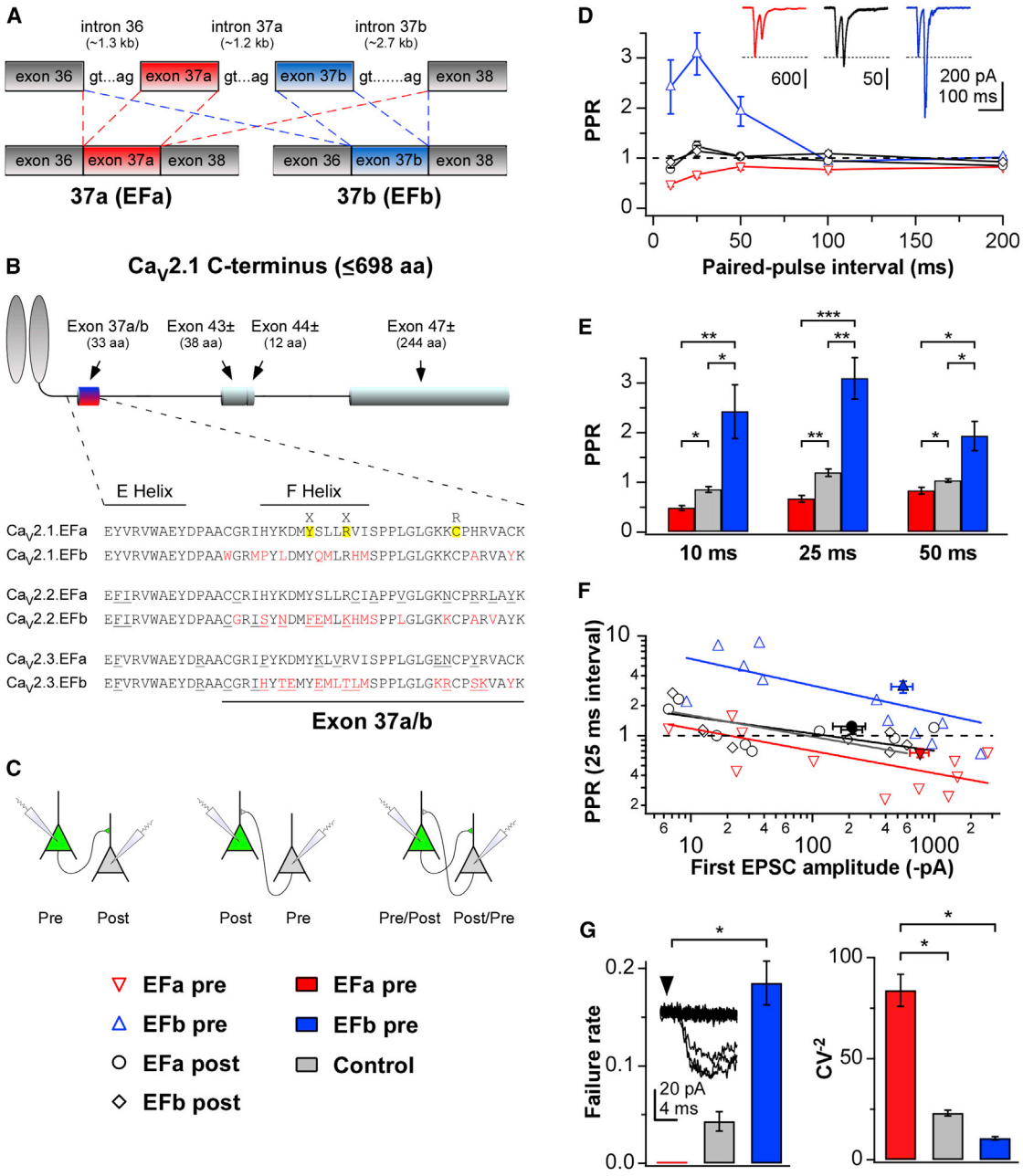

Figure 1. Presynaptically Expressed Ca$_V$2.1[EFa] and Ca$_V$2.1[EFb] Differentially Regulate Short-Term Synaptic Plasticity

(A) Postulated mechanism of alternative splicing for exon 37a/b. Either exon 37a or 37b is included in the final mRNA, resulting in two mutually exclusive splice isoforms of an EF-hand-like domain (EFa and EFb). Scheme adapted from Soong et al. (2002).

(B) Top: cartoon of the cytoplasmic C terminus of the human Ca$_V$2.1 α_1 subunit drawn to scale. Exons 37a/b (red/blue) are depicted in relationship to the other alternative exons. Bottom: alternative splicing of exons 37a/b is conserved within Ca$_V$2 channels. Differences between splice isoforms are indicated in red, and those between Ca$_V$2.1, Ca$_V$2.2, and Ca$_V$2.3 are underscored. Residues highlighted in yellow have been found mutated in patients with episodic ataxia type 2 (Graves et al., 2008; Mantuano et al., 2010).

(C) Recording configurations in primary hippocampal cultures for experiments as in (D–G). Green indicates transfected neurons.

(D) Paired-pulse ratios (PPRs) versus paired-pulse intervals for paired recordings between hippocampal pyramidal neurons. Presynaptic expression of Ca$_V$2.1 [EFa] favors paired-pulse depression (PPD; EFa pre, red, n = 11 recordings), while presynaptic expression of Ca$_V$2.1[EFb] induces strong paired-pulse facilitation (PPF; EFb pre, blue, n = 11 recordings); a PPR close to 1 is observed when either Ca$_V$2.1[EFa] or Ca$_V$2.1[EFb] is expressed postsynaptically (EFa post and EFb post, black, n = 8 recordings each). Inset: representative EPSCs for the 25 ms paired-pulse interval. Traces are averages of three trials (red, EFa pre; black, EFa post; blue, EFb pre).

(E) Summary of PPRs at 10, 25, and 50 ms paired-pulse intervals, showing PPD for EFa pre and PPF for EFb pre. Because no differences were detected between EFa post and EFb post in (D), the two groups were pooled (control; *$p < 0.04$, **$p \leq 0.01$, and ***$p < 0.0001$).

(legend continued on next page)

neurons upregulate selectively $Ca_v2.1$[EFa], the splice isoform displaying the higher synaptic efficacy, thus effectively counteracting the decrease in network activity.

RESULTS

$Ca_v2.1$ Splice Variants Are Targeted to Presynaptic Boutons Where They Differentially Regulate P_r and Short-Term Synaptic Plasticity

In order to compare the relative contributions of $Ca_v2.1$[EFa] and $Ca_v2.1$[EFb] splice isoforms to synaptic transmission, we first took an overexpression approach. Confocal imaging showed that both isoforms were efficiently targeted to axons and presynaptic boutons in primary hippocampal neurons (Figure S1), where they partially replaced endogenous $Ca_v2.1$ channels (Figure S2). The level of co-localization with the presynaptic cytomatrix protein bassoon was overall higher for $Ca_v2.1$[EFa] than for $Ca_v2.1$[EFb] (Figure S1D). We next asked whether the exogenously expressed $Ca_v2.1$ splice variants affected presynaptic Ca^{2+} transients. First, we used a presynaptically localized Ca^{2+} indicator, SyGCaMP3, in which GCaMP3 was fused to synaptophysin (Dreosti et al., 2009), to qualitatively monitor changes in presynaptic Ca^{2+} levels (see Supplemental Experimental Procedures). Expression of either splice isoform strongly increased presynaptic Ca^{2+} signals, with $Ca_v2.1$[EFa] inducing larger transients than $Ca_v2.1$[EFb] (Figures S3A–S3C). To quantitatively compare presynaptic Ca^{2+} signals between the two isoforms, we used Fluo-4, a Ca^{2+} indicator providing a linear readout of action potential (AP)-evoked presynaptic Ca^{2+} influx (see Supplemental Experimental Procedures). In response to two successively applied APs, $Ca_v2.1$[EFb] induced a small (~10%) but significantly higher facilitation of presynaptic Ca^{2+} transients relative to $Ca_v2.1$[EFa] (Figures S3D–S3G). If we consider that there is a steep power dependence of release probability (P_r) on Ca^{2+} entry, the observed differences in presynaptic Ca^{2+} transients between $Ca_v2.1$[EFa] and $Ca_v2.1$[EFb] could also produce differences in the efficacy of neurotransmitter release and short-term synaptic plasticity.

In order to determine whether the two splice isoforms differentially regulated synaptic efficacy and plasticity, we performed paired recordings from monosynaptically connected primary hippocampal pyramidal neurons with only one of the two neurons transfected with either $Ca_v2.1$[EFa] or $Ca_v2.1$[EFb] (Figure 1C). Strikingly, presynaptic expression of the two splice isoforms affected paired-pulse ratio (PPR) of evoked excitatory postsynaptic currents (EPSCs) in opposite directions. $Ca_v2.1$[EFa] promoted paired-pulse depression (PPD), with a concomitant decrease in failure rate and an increase in CV^{-2} (coefficient of variation) of EPSC amplitudes (Figures 1D–1G), suggesting an increase in P_r (Chavez-Noriega and Stevens, 1994). In contrast, $Ca_v2.1$[EFb] induced prominent paired-pulse facilitation (PPF), increased failure rate, and decreased CV^{-2} (Figures 1D–1G). Altogether, these changes were consistent with $Ca_v2.1$[EFa] enhancing and $Ca_v2.1$[EFb] reducing P_r.

To corroborate the changes in P_r by $Ca_v2.1$ splice isoforms, we next used the NMDA receptor (NMDAR) open channel blocker MK-801, whose rate of block of NMDAR EPSCs is indicative of P_r, with higher P_r synapses producing a faster rate of decay (Hessler et al., 1993; Rosenmund et al., 1993). As shown in Figure 2, expression of $Ca_v2.1$[EFa] and $Ca_v2.1$[EFb] differentially affected the progressive block of NMDAR responses by MK-801. Although both splice isoforms accelerated the MK-801-dependent block of synaptic NMDAR EPSCs, $Ca_v2.1$[EFa] was more effective than $Ca_v2.1$[EFb]. In particular, the number of stimuli necessary to achieve a 50% block of NMDAR EPSCs with MK-801 was significantly reduced only by $Ca_v2.1$[EFa] (3.50 ± 0.62, 9.29 ± 0.72, and 6.56 ± 0.80 stimuli for $Ca_v2.1$[EFa], control, and $Ca_v2.1$[EFb], respectively; Figure 2C), indicating that neurons expressing $Ca_v2.1$[EFa] exhibit overall higher P_r than naive neurons.

Collectively, these findings suggest that $Ca_v2.1$ splice isoforms differentially regulate P_r and short-term synaptic plasticity.

$Ca_v2.1$ Splice Isoforms Are Differentially Coupled to the Neurotransmitter Release Machinery

Motivated by previous findings in which the efficacy of AP-driven neurotransmitter release is affected by the localization of Ca^{2+} channels at the active zone (AZ; Kaeser et al., 2011; Mochida et al., 1996; Wu et al., 1999), we examined whether the observed differences in synaptic efficacy between $Ca_v2.1$[EFa] and $Ca_v2.1$[EFb] reflected a differential functional coupling of the two isoforms to the neurotransmitter release machinery. If the lower P_r and strong PPF associated with $Ca_v2.1$[EFb] were due to a less efficient coupling of this channel to the release machinery, then the slow Ca^{2+} chelator EGTA should be more effective in intercepting Ca^{2+} and inhibiting exocytosis for $Ca_v2.1$[EFb] than for $Ca_v2.1$[EFa]. We tested this hypothesis with two complementary approaches. First, we used synaptophysin-pHluorin (SypHy) to directly monitor vesicle turnover before and after application of EGTA-AM under conditions that deplete the readily releasable

(F) PPR at 25 ms interval versus first EPSC amplitude showing that the differences in PPR between the two splice isoforms are observed across a broad range of EPSC amplitudes; lines are linear regression fits of the log-transformed data (black line, EFa post; gray line, EFb post). Open symbols represent individual recordings, filled symbols population averages.

(G) Left, presynaptic expression of $Ca_v2.1$[EFb] induces a high failure rate of synaptic transmission. Failures were never observed with presynaptic $Ca_v2.1$[EFa] (n = 11 pairs), but they were present in 2 of 16 control recordings, in which the presynaptic neuron was untransfected (failure rate, amplitude without failures of the first synchronous EPSC, and median amplitude of the asynchronous release: 0.63, −7.1 pA, and −8.5 pA [21 events] for the first pair and 0.06, −6.6 pA, −6.5 pA [5 events] for the second pair) and in 5 of 11 recordings with presynaptic $Ca_v2.1$[EFb] (failure rate, amplitude without failures of the first synchronous EPSC, and median amplitude of the asynchronous release: 0.07, −16.7 pA, and −19.4 pA [44 events] for the first pair; 0.07, −38.9 pA, and −21.9 pA [38 events] for the second pair, 0.78, −36.5 pA; −30.1 pA [9 events] for the third pair; 0.67, −27.2 pA, and −28.1 pA [11 events] for the fourth pair; and 0.46, −9.2 pA, and −8.5 pA [8 events] for the fifth pair; *$p < 0.05$). Inset: 17 consecutive EPSCs for an EFb pre pair, showing high failure rate. Right: summary of the effects of $Ca_v2.1$ splice isoforms on the coefficient of variation (CV) of evoked EPSCs. Presynaptic $Ca_v2.1$[EFa] induces a significant increase in CV^{-2} relative to presynaptic untransfected neurons (control) and presynaptic $Ca_v2.1$[EFb] (*$p < 0.05$), consistent with an increase in P_r.

Data are presented as mean ± SEM. See also Figures S1–S3.

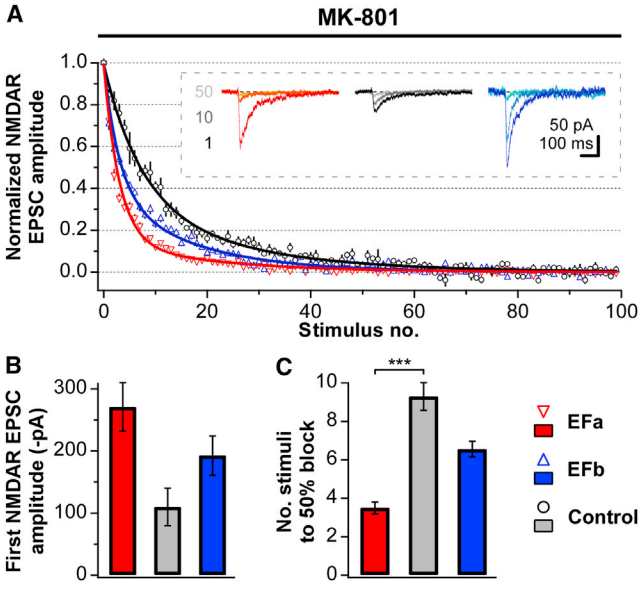

Figure 2. $Ca_v2.1$[EFa] and $Ca_v2.1$[EFb] Differentially Regulate P_r

(A) Plot of the effects of the open-channel blocker MK-801 (5 μM) on NMDAR currents in primary hippocampal pyramidal neurons; recording configuration as in Figure 1. The decay rates of NMDAR EPSCs were fit by the sum of two decaying exponentials ($f[x] = A_{fast}{}^{*}\exp[-x/\tau_{fast}] + A_{slow} \times \exp[-x/\tau_{slow}]$). The progressive block of NMDAR responses by MK-801 is accelerated by presynaptic expression of $Ca_v2.1$[EFa] (red, n = 10 recordings) and, to a lesser extent, by that of $Ca_v2.1$[EFb] (blue, n = 9 recordings), compared with control (black, n = 7 recordings). Inset: representative NMDAR EPSCs for the 1st, 10th, and 50th stimulus.

(B) Mean amplitude of first NMDAR EPSCs.

(C) Summary of the number of stimuli necessary to achieve a 50% block of NMDAR EPSCs with MK-801 for experiments as in (A) (***$p < 0.001$).

Data are presented as mean ± SEM. See also Figures S1–S3.

pool (RRP; 40 APs at 20 Hz). We chose concentrations and incubation times of the chelator that produced ~50% reduction in exocytosis in control neurons (Hoppa et al., 2012). EGTA-AM decreased vesicle release by nearly 70% in boutons expressing $Ca_v2.1$[EFb], whereas it had little effect in the presence of $Ca_v2.1$[EFa] (Figures 3A and 3B).

Because multiple Ca^{2+}-dependent mechanisms are at work in response to trains of APs, we next used electrophysiology to examine the effects of EGTA on EPSCs evoked by individual APs. We found that $Ca_v2.1$[EFa] minimized while $Ca_v2.1$[EFb] enhanced the EGTA-dependent decrease in the amplitude of EPSCs (Figure 3C). EGTA also abolished selectively the PPF observed in the presence of $Ca_v2.1$[EFb] (Figure 3D), suggesting that facilitation was largely driven by accumulation of residual free Ca^{2+} in neurons expressing $Ca_v2.1$[EFb].

Taken together, these findings support a model whereby $Ca_v2.1$[EFa] and $Ca_v2.1$[EFb] are differentially coupled to the neurotransmitter release machinery.

Endogenous $Ca_v2.1$ Splice Isoforms Control Presynaptic Ca^{2+} Influx and Vesicle Release

Thus far, we have taken an overexpression approach to probe the differential properties of the two $Ca_v2.1$ splice variants. We next addressed whether the effects of exogenously expressed $Ca_v2.1$[EFa] and $Ca_v2.1$[EFb] reflected the function of the respective endogenous $Ca_v2.1$ isoforms. First, we developed isoform-specific microRNAs (miRs) to knockdown selectively $Ca_v2.1$[EFa] or $Ca_v2.1$[EFb] (Figure S4A and Supplemental Experimental Procedures) and assessed by confocal microscopy (Figures 4A–4F) that silencing either $Ca_v2.1$[EFa] or $Ca_v2.1$[EFb] effectively reduced immunofluorescence signal of total $Ca_v2.1$ in presynaptic boutons (−40 ± 8.1% and −50 ± 7.6% for miR EFa1 and miR EFa3, which both target $Ca_v2.1$[EFa], and −52 ± 7.1% for miR EFb2, which targets $Ca_v2.1$[EFb]; Figures 4A and 4B). Notably, knockdown of $Ca_v2.1$[EFb] resulted in an increase in the extent of co-localization of $Ca_v2.1$ with the presynaptic marker bassoon (Figures 4A and 4D), suggesting that endogenous $Ca_v2.1$[EFa] is more tightly localized with presynaptic scaffold proteins than $Ca_v2.1$[EFb].

To determine whether the reduction in presynaptic expression of $Ca_v2.1$ was accompanied by changes in Ca^{2+} transients, we used the highly sensitive presynaptic Ca^{2+} indicator SyGCaMP6s (see Supplemental Experimental Procedures), because an overall decrease in Ca^{2+} entry was expected. Indeed, knockdown of either $Ca_v2.1$[EFa] or $Ca_v2.1$[EFb] decreased AP-triggered presynaptic Ca^{2+} signals across a broad range of stimulus intensities (Figures S4D–S4F). Moreover, targeting both splice isoforms nearly abolished measurable Ca^{2+} transients in response to one or two APs (Figures S4D and S4F), in further support of the effectiveness of our knockdown approach.

Next, we tested if the differences in the localization of $Ca_v2.1$ splice isoforms (Figures 4A and 4D) were associated with differences in their function at the synapse. As measured by the SypHy assay, knockdown of $Ca_v2.1$[EFa] significantly increased the sensitivity of vesicle turnover to EGTA-AM, (~80% reduction in SypHy responses relative to baseline versus ~50% in controls); in contrast, knockdown of $Ca_v2.1$[EFb] did not increase EGTA sensitivity (Figures 5, S4B, and S4C). These findings therefore suggest that endogenous $Ca_v2.1$[EFb] is the splice variant more sensitive to EGTA in naive conditions.

Endogenous $Ca_v2.1$ Splice Isoforms Differentially Regulate Short-Term Synaptic Plasticity in Intact Hippocampal Circuits

To investigate whether alternative splicing at the EF-hand-like domain of $Ca_v2.1$ is important for short-term synaptic plasticity in intact brain circuits, we knocked down either $Ca_v2.1$[EFa] or $Ca_v2.1$[EFb] in the hippocampus, where both splice isoforms are expressed at comparable levels (42.9 ± 0.8% and 57.1 ± 0.8% transcript expression levels for $Ca_v2.1$[EFa] and $Ca_v2.1$[EFb], respectively; see Supplemental Experimental Procedures). To monitor synaptic transmission selectively at connections where presynaptic neurons were knocked down for the $Ca_v2.1$ splice variants, we stereotactically injected adeno-associated viruses (AAVs) expressing $Ca_v2.1$ splice isoform-specific miRs along with the ultrafast channelrhodopsin ChETA (Gunaydin et al., 2010) fused to the fluorescent protein TdTomato into area CA3 of the rat hippocampus (Figures 6A, 6B, and S5A and Supplemental Experimental Procedures).

We then prepared acute hippocampal slices from AAV-injected animals and evoked AP-dependent, AMPAR-mediated

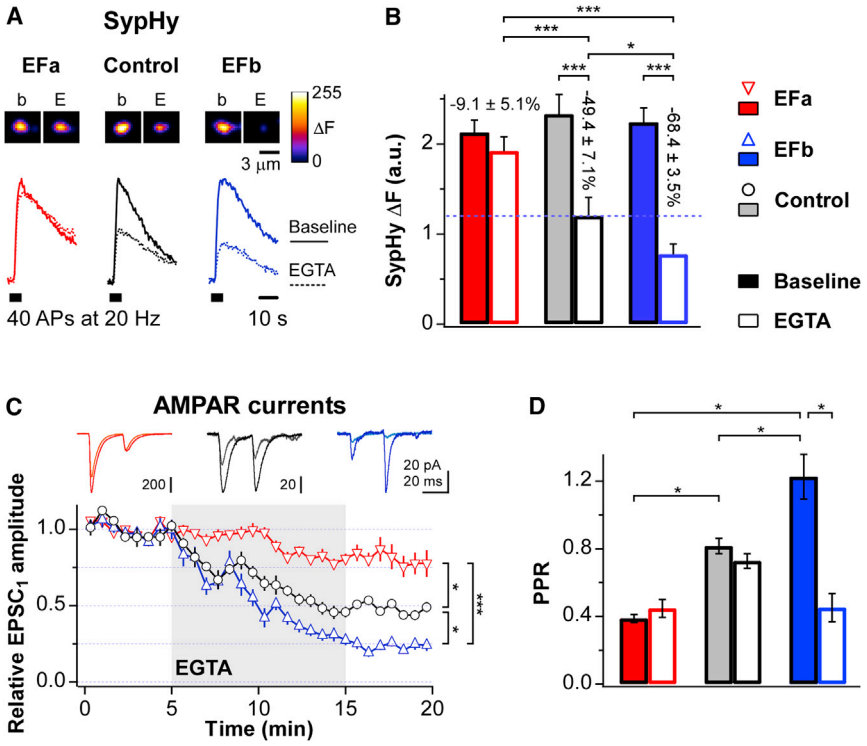

Figure 3. $Ca_v2.1$[EFa] and $Ca_v2.1$[EFb] Are Differentially Coupled to the Neurotransmitter Release Machinery

(A) SypHy responses for $Ca_v2.1$[EFa], $Ca_v2.1$[EFb], and control to 40 APs at 20 Hz before (continuous line) and after (dotted line) EGTA-AM application (200 μM; loaded for 90 s, followed by 10 min wash). Traces are normalized to pre-EGTA responses in control. Inset: individual boutons for the three conditions (b, pre-EGTA; E, post-EGTA).

(B) Summary of experiments as in (A) showing that sensitivity of vesicle turnover to EGTA is decreased by $Ca_v2.1$[EFa] and increased by $Ca_v2.1$[EFb] (n = 9, 9, and 7 independent experiments for $Ca_v2.1$[EFa], $Ca_v2.1$[EFb], and control, respectively; *p < 0.05 and ***p < 0.001).

(C) Time course of the effects of EGTA-AM (50 μM) on the amplitude of the first of two EPSCs evoked in primary hippocampal pyramidal neurons. Recording configuration is as in Figure 1, with a 25 ms paired-pulse interval. Gray area indicates the period of EGTA-AM application. Relative to controls (black, n = 10 recordings), presynaptic expression of $Ca_v2.1$[EFa] (red, n = 6 recordings) and $Ca_v2.1$[EFb] (blue, n = 8 recordings) minimizes and accentuates the EGTA-dependent decrease in AMPAR EPSCs, respectively (*p < 0.05 and ***p < 0.001). This is consistent with $Ca_v2.1$[EFa] and $Ca_v2.1$[EFb] being tightly and loosely coupled to the release machinery, respectively. Inset: representative EPSC pairs before (darker) and after (lighter traces) EGTA-AM application.

(D) Summary of PPRs under basal conditions (filled bars) and after application of EGTA-AM (open bars) from experiments in (C). Application of EGTA-AM abolishes PPF that accompanies presynaptic expression of $Ca_v2.1$[EFb], suggesting an involvement of residual free Ca^{2+} in the $Ca_v2.1$[EFb]-dependent facilitation (*p < 0.05).

Data are presented as mean ± SEM. See also Figures S1–S3.

EPSCs in CA1 pyramidal neurons by stimulating CA3 somata with brief blue light pulses (2 ms long; Figures 6C, S5B, and S5C). We found that knockdown of $Ca_v2.1$ splice isoforms affected responses to paired-pulse stimulation in opposite directions: knockdown of $Ca_v2.1$[EFa] boosted PPF, whereas knockdown of $Ca_v2.1$[EFb] abolished it (Figures 6D, 6E, and S5D).

Synaptic transmission is mediated mostly by P/Q-type and N-type Ca^{2+} channels at these synapses (Reid et al., 1998; Scholz and Miller, 1995). To rule out the possibility that some of the effects we observed upon knockdown of P/Q-type $Ca_v2.1$ splice isoforms were due to a compensatory upregulation of N-type channels, we repeated the above experiments in the presence of ω-conotoxin GVIA to block N-type channels. As shown in Figures S5E and S5F, the increase in PPR with miRs directed against $Ca_v2.1$[EFa] and its decrease with miR against $Ca_v2.1$[EFb] were still observed after blockade of N-type channels. Taken together, these data suggest that $Ca_v2.1$[EFa] and $Ca_v2.1$[EFb] splice variants shape short-term plasticity at hippocampal synapses.

Neurons Regulate the Expression of $Ca_v2.1$[EFa] in a Homeostatic Fashion

We next investigated whether hippocampal neurons modulate the balance between the two $Ca_v2.1$ splice variants to regulate synaptic efficacy in an activity-dependent manner. We turned to a presynaptic form of homeostatic plasticity whereby neurons scale up presynaptic efficacy to counterbalance a chronic reduction in network excitability. This form of plasticity depends, at least in part, on changes in presynaptic Ca^{2+} and $Ca_v2.1$ channels (Frank et al., 2006; Jakawich et al., 2010; Zhao et al., 2011).

First, we tested if inducing homeostatic plasticity affected the expression of $Ca_v2.1$ splice isoforms. As shown in Figure 7A, two different activity deprivation protocols commonly used to induce homeostatic plasticity in primary cultures scaled up the transcript of $Ca_v2.1$[EFa] but not that of $Ca_v2.1$[EFb], with the effects peaking at 24 hr. We next determined whether the activity-dependent changes at the mRNA level were reflected in changes in protein content for $Ca_v2.1$ at the synapse. Chronic activity deprivation scaled up synaptic $Ca_v2.1$ in control conditions (Figures 7B and 7C), in agreement with previous observations (Lazarevic et al., 2011). Remarkably, this effect was blocked by knockdown of $Ca_v2.1$[EFa] but not by that of $Ca_v2.1$[EFb] (Figures 7B and 7C), suggesting that only $Ca_v2.1$[EFa] expression is regulated by activity and that the synaptic increase in $Ca_v2.1$ content upon activity deprivation is due mainly to $Ca_v2.1$[EFa].

To investigate changes in presynaptic function directly, we examined activity-dependent vesicle turnover by monitoring the uptake of an antibody against the luminal domain of synaptotagmin (Stg). In line with previous reports (Jakawich et al., 2010), we found that Stg uptake was dependent on P/Q-type

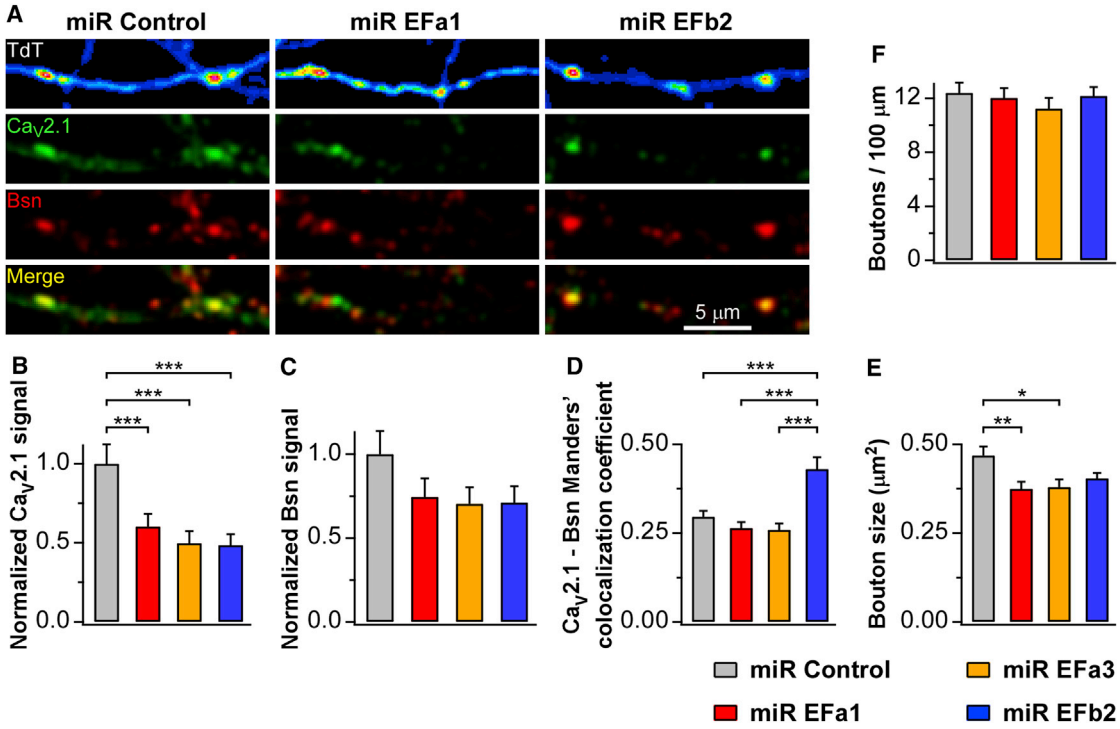

Figure 4. Splice Isoform-Specific MicroRNAs Reduce Endogenous $Ca_V2.1$ Channels at Presynaptic Boutons

(A) Confocal microscopy images of primary hippocampal axons expressing TdTomato and the indicated microRNAs (miRs). Bassoon (Bsn) and TdTomato (TdT) were used as presynaptic and morphological markers, respectively. $Ca_V2.1$ was detected with an antibody recognizing both splice isoforms.

(B) Quantification of experiments as in (A) indicating that knockdown of either $Ca_V2.1$[EFa] (miR EFa1, red, or miR EFa3, orange) or $Ca_V2.1$[EFb] (miR EFb2, blue) reduces endogenous $Ca_V2.1$ in axons to a similar extent, relative to the negative control (miR control, gray).

(C) Quantification of the effects of the indicated miRs on bassoon expression.

(D) Mander's co-localization coefficient for $Ca_V2.1$ with bassoon is selectively and largely increased by knockdown of $Ca_V2.1$[EFb], suggesting that endogenous $Ca_V2.1$[EFa] co-localizes with bassoon better than $Ca_V2.1$[EFb].

(E and F) Quantification of the effects of the indicated miRs on bouton size (E) and number (F) (n = 32, 41, 33, and 38 fields of view for miR control, miR EFa1, miR EFa3, and miR EFb2, respectively; *p < 0.05, **p < 0.01, and ***p < 0.001).

Data are presented as mean ± SEM. See also Figure S4.

channels, because ω-agatoxin TK, a blocker of these channels, reduced the uptake under basal (untreated) and activity-deprived conditions (CNQX/DAPV; Figures 7D and 7E). Notably, although knockdown of either splice variant reduced Stg uptake under basal conditions, only knockdown of $Ca_V2.1$[EFa] prevented the increase in Stg uptake that followed activity deprivation (Figures 7B, 7D, and 7E). Altogether, these findings indicate that homeostatic upregulation of presynaptic release induced by activity deprivation is selectively dependent on $Ca_V2.1$[EFa], the splice isoform exhibiting higher synaptic efficacy.

DISCUSSION

We have combined electrophysiological recordings with optogenetic stimulation, along with imaging of presynaptic Ca^{2+} and vesicle turnover, to assess how two major mutually exclusive splice isoforms of P/Q-type channels ($Ca_V2.1$[EFa] and $Ca_V2.1$[EFb]; Figures 1A and 1B) regulate excitatory synaptic transmission and presynaptic plasticity in hippocampal neurons. In particular, the use of optogenetics to selectively stimulate neurons expressing isoform-specific miRs enabled us to examine the role of alternatively spliced $Ca_V2.1$ variants in intact hippocampal circuits. Such a strategy may be generally applicable for studies of the physiological significance of presynaptically expressed proteins in synaptic transmission.

We propose that P/Q-type $Ca_V2.1$ channels do not constitute a uniform population with respect to their efficacy for eliciting vesicle release. In particular, the two mutually exclusive $Ca_V2.1$[EFa] and $Ca_V2.1$[EFb] isoforms play unique roles in shaping presynaptic plasticity: $Ca_V2.1$[EFa] is more effective in supporting neurotransmitter release and promotes PPD, while $Ca_V2.1$[EFb] displays a lower synaptic efficacy that favors PPF (Figures 7F and S7). Our findings are in line with a large body of evidence supporting the following model: at high-P_r synapses displaying PPD, VGCCs are tightly localized at the presynaptic AZ, where they increase Ca^{2+} locally, thus driving vesicle release effectively in response to a single AP; in contrast, at low-P_r synapses with a prominent PPF, VGCCs are farther away from the AZ, thus boosting the residual Ca^{2+} that facilitates release during repetitive stimulations but contributing little to the Ca^{2+} signal at the AZ in response to single APs (Eggermann et al., 2012; Hoppa et al., 2012; Kaeser et al., 2011; Mochida et al., 1996; Vyleta and Jonas, 2014; Wu et al., 1999).

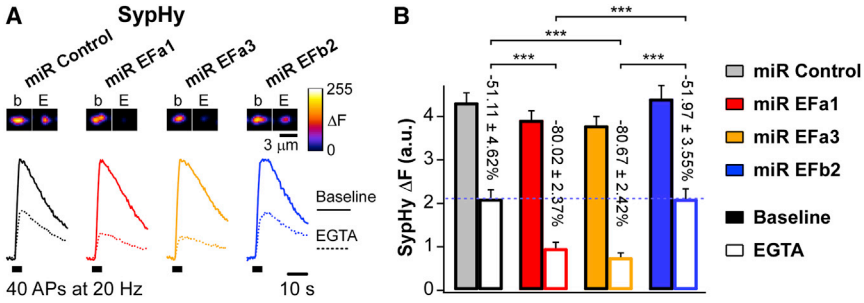

Figure 5. Knockdown of $Ca_v2.1$[EFa] Selectively Increases the Sensitivity of Vesicle Release to EGTA

(A) SypHy responses for miR control, miR EFa1, miR EFa3, and miR EFb2 to 40 APs at 20 Hz before (continuous line) and after (dotted line) EGTA-AM application (200 μM; loaded for 90 s, followed by 10 min wash). Traces are normalized to pre-EGTA responses in miR control. Inset: individual boutons for the four conditions (b, pre-EGTA; E, post-EGTA).

(B) Summary of experiments as in (A) (n = 10, 13, 12, and 11 independent experiments for miR control, miR EFa1, miR EFa3, and miR EFb2, respectively; ***$p < 0.001$). Sensitivity to EGTA is selectively increased by knockdown of $Ca_v2.1$[EFa].

Data are presented as mean ± SEM. See also Figure S4.

In our overexpression experiments, we used $Ca_v2.1$ channels devoid of the long C-terminal exon 47 (Figure 1B) because we wanted to investigate the functional consequences of alternative splicing at exon 37a/b while trying to minimize the interference by other domains. Inclusion of the C-terminal exon 47 generates $Ca_v2.1$ channels with additional 244 amino acids that carry motifs for binding to the PDZ domains of Mint1 and RIM proteins (Kaeser et al., 2011; Maximov et al., 1999) and to the SH3 domains of RIM-binding proteins (Davydova et al., 2014; Hibino et al., 2002). Although these interactions are important to target P/Q- and N-type Ca^{2+} channels to vesicle release sites, P/Q-type channels devoid of exon 47 are abundant in the brain (Soong et al., 2002) and can accumulate efficiently at synapses, as previously documented (Cao and Tsien, 2010; Hu et al., 2005; Schneider et al., 2015) and as we report here (Figures S1–S3).

Additional interacting domains, such as those in the intracellular loop between domains II and III of $Ca_v2.1$ and $Ca_v2.2$ channels, which bind to SNARE proteins (Mochida et al., 1996; Rettig et al., 1996; Sheng et al., 1994), and those in the intracellular loop between domains I and II of VGCCs, which bind to auxiliary β subunits (Kiyonaka et al., 2007; Pragnell et al., 1994), play a key role in anchoring VGCCs at presynaptic sites. Specifically, auxiliary β subunits form a bridge between VGCC α_1 subunits and the AZ protein RIM1 (Kiyonaka et al., 2007), thus effectively linking VGCCs to the presynaptic cytomatrix. Indeed, we find that the auxiliary subunit β4 is required for efficient targeting of exogenous $Ca_v2.1$[EFa] and $Ca_v2.1$[EFb] to axons (Figure S1).

The differences in synaptic efficacy between $Ca_v2.1$[EFa] and $Ca_v2.1$[EFb] (Figures 1, 2, 6, S5, and S6) are likely due to a differential organization of the two splice isoforms at presynaptic sites, as we find marked differences in their presynaptic localization (Figures 4 and S1) and in their sensitivity to the slow Ca^{2+} chelator EGTA (Figures 3 and 5). The EF-hand-like domains encoded by exons 37a and 37b might represent additional interacting domains important for the precise and differential positioning of P/Q-type channel isoforms relative to the neurotransmitter release machinery.

Although our experiments suggest that the primary difference between $Ca_v2.1$[EFa] and $Ca_v2.1$[EFb] lies in their spatial relationship to fuse-competent vesicles, we cannot rule out that differences in their biophysical properties might also contribute to setting synaptic efficacy at central synapses. The $Ca_v2.1$[EFb]-dependent facilitation of synaptic transmission (Figures 1 and 6), however, could not be predicted by experiments in heterologous expression systems, where $Ca_v2.1$[EFb] shows little or no Ca^{2+}-dependent facilitation of the channel (Chaudhuri et al., 2004). Differences in the availability of Ca^{2+}-binding proteins regulating Ca^{2+}-dependent facilitation might however result in VGCCs with divergent functional properties between presynaptic boutons and heterologous expression systems (Lautermilch et al., 2005; Lee et al., 2002).

Alternative splicing at exons 37a and 37b is conserved across P/Q-, N-, and R-type Ca^{2+} channels (Figure 1B; Gray et al., 2007), suggesting that it might represent a common mechanism to regulate the synaptic function of these VGCCs. Regarding N-type Ca^{2+} channels, the $Ca_v2.2$[EFa] isoform is selectively expressed in capsaicin-responsive nociceptors of dorsal root ganglia (Bell et al., 2004), where it mediates thermal nociception (Altier et al., 2007; Andrade et al., 2010). In contrast, $Ca_v2.2$[EFb] is the isoform abundant throughout the nervous system (Bell et al., 2004).

Considering that the expression of $Ca_v2.1$[EFa] and $Ca_v2.1$[EFb] splice isoforms varies during development (Vigues et al., 2002), across brain regions (Bourinet et al., 1999; Chaudhuri et al., 2004), and in response to changes in neuronal network activity (Figures 7A–7C), their differential efficacy to promote synaptic transmission (Figures 2 and S6) likely contributes to the intersynaptic variability in P_r and short-term synaptic plasticity. For instance, the increase in $Ca_v2.1$[EFa] expression that occurs during development (Vigues et al., 2002) correlates with the tightening of the coupling between VGCCs and Ca^{2+} sensor observed during synapse maturation (Eggermann et al., 2012). Conversely, $Ca_v2.1$[EFb] predominates in neurons forming highly facilitating synapses, such as hippocampal granule cells (Vigues et al., 2002).

We found that the relative abundance of the two splice isoforms at the synapse is regulated in a homeostatic fashion to adapt presynaptic strength to changes in neuronal network activity (Figures 7 and S7). Specifically, hippocampal neurons selectively increase the expression of $Ca_v2.1$[EFa] in response to activity deprivation. Because this splice isoform drives the higher synaptic efficacy of the two, it can effectively support homeostatic upregulation of presynaptic release. This finding provides therefore a clear molecular basis for the previous

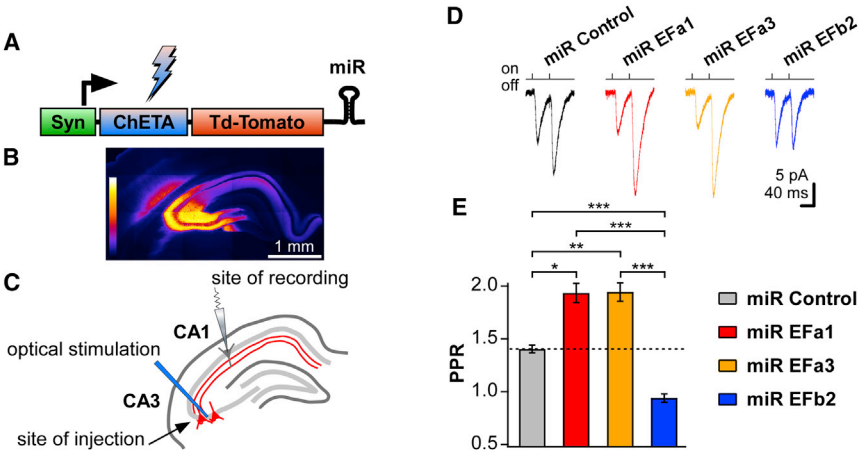

Figure 6. Assessing the role of $Ca_v2.1$[EFa] and $Ca_v2.1$[EFb] in the Native Hippocampus by Targeted Stimulation of Knocked-Down Neurons with Optogenetics

(A) Scheme of AAV constructs used for in vivo infection, containing a synapsin promoter (Syn), the ultrafast channelrhodopsin ChETA fused to TdTomato and, in the 3′UTR, $Ca_v2.1$ splice isoform-specific miRs.

(B) Hippocampal section showing that TdTomato fluorescence is limited to the CA3 region and its projections.

(C) Experimental configuration: laser beam was directed onto CA3 somata, and patch-clamp recordings were performed from CA1 pyramidal neurons.

(D) Two-millisecond-long blue light pulses shone at 20 Hz evoke EPSCs whose PPF is increased by miRs targeting $Ca_v2.1$[EFa] and abolished by miR for $Ca_v2.1$[EFb].

(E) Summary of PPRs for experiments as in (D) showing an increase in PPF for miR EFa1 and miR EFa3 and a decrease for miR EFb2, relative to miR control (n = 11, 9, 9, and 10 recordings for miR control, miR EFa1, miR EFa3, and miR EFb2, respectively; *p = 0.02, **p = 0.01, and ***p < 0.0004).
Data are presented as mean ± SEM. See also Figures S4 and S5.

observations implicating VGCC-mediated Ca^{2+} signals and their upregulation in presynaptic homeostatic plasticity (Frank et al., 2006; Jakawich et al., 2010; Lazarevic et al., 2011; Zhao et al., 2011) and highlights the importance of alternative splicing of P/Q-type Ca^{2+} channels in shaping presynaptic function in an activity-dependent manner.

In summary, previous studies have described that different VGCC types are differentially recruited to the AZ, with P/Q-type channels generally being more effective than N- and R-type channels in eliciting neurotransmitter release (Wu et al., 1999), and that auxiliary subunits can effectively control the trafficking and gating of VGCCs. In particular, auxiliary $\alpha_2\delta$ subunits affect the coupling between synaptic VGCCs and the RRP at hippocampal synapses (Hoppa et al., 2012, but see Schneider et al., 2015). Our findings show that also the balance between two mutually exclusive splice variants of a pore-forming VGCC α_1 subunit shapes synaptic transmission and plasticity. Importantly, hippocampal neurons regulate the relative abundance of the two splice isoforms in an activity-dependent manner. Considering that alternative splicing of α_1 subunits is prominent in the brain (Lipscombe et al., 2013; Simms and Zamponi, 2014; Soong et al., 2002), it is tempting to speculate that a combinatorial splicing code might exist to match the expression of multiple VGCC splice isoforms to the specific needs of synaptic transmission under different activity states.

EXPERIMENTAL PROCEDURES

RNAi

Splice isoform-specific miRs for rat $Ca_v2.1$[EFa] (miR EFa1: TCCTTATAGT GAATGCGGCCG; miR EFa3: TTGCAAGCAACCCTATGAGGA) and $Ca_v2.1$ [EFb] (miR EFb2: ATCTGATACATGTCCGGGTAA) were generated using the BLOCK-iT kit (Invitrogen) and validated by western blotting and RT-qPCR. As a negative control (miR control), we used the pcDNA6.2-GW/EmGFP-miR-neg plasmid from the kit containing a sequence that does not target any known vertebrate gene. Detailed methods are described in the Supplemental Information.

In Vivo Knockdown

AAV1/2 expressing the ultrafast channelrhodopsin ChETA, TdTomato, and $Ca_v2.1$ splice isoform-specific miRs were injected into the CA3 region of P18 rats, with coordinates of (A-P/M-L/D-V from Bregma) −2.6/ ± 2.9/−2.9, as detailed in Supplemental Experimental Procedures.

Electrophysiology in Primary Cultures

Whole-cell recordings were performed from pyramidal neurons of rat hippocampal cultures, continuously perfused with aCSF containing 140 mM NaCl, 2.5 mM KCl, 2.2 mM $CaCl_2$, 2.3 mM $MgCl_2$, 10 mM D-glucose, and 10 mM HEPES-NaOH (pH 7.38, osmolarity adjusted to 290 mOsm). A $GABA_A$ receptor blocker (100 μM picrotoxin) was routinely included in the aCSF. For EGTA-AM experiments, $CaCl_2$ was raised to 2.5 mM and $MgCl_2$ lowered to 1.5 mM. To isolate NMDAR-mediated EPSCs, $CaCl_2$ and $MgCl_2$ were lowered to 1.5 and 0.1 mM, respectively, and aCSF was supplemented with an NMDAR co-agonist (20 μM glycine) and an AMPAR blocker (2 μM NBQX). The intracellular solution contained 100 mM K-gluconate, 5 mM K-glutamate, 17 mM KCl, 5 mM NaCl, 0.5 mM EGTA, 5 mM $MgCl_2$, 4 mM K_2-ATP, 0.5 mM Na_3-GTP, 20 mM K_2-creatine phosphate, and 10 mM HEPES-KOH (pH 7.28, osmolarity adjusted to 280 mOsm). Pre- and postsynaptic neurons were voltage-clamped at −70 and −50 mV for AMPAR- and NMDAR-mediated EPSC recordings, respectively; in order to evoke synaptic transmission, unclamped Na^+ spikes were elicited in the presynaptic neuron by delivering one or two depolarizing stimuli (+30 mV, 2 ms long) at various interstimulus intervals (see Supplemental Experimental Procedures).

Electrophysiology and Optogenetics in Acute Brain Slices

All experiments were carried out in accordance with the guidelines established by the European Communities Council (Directive 2010/63/EU of March 4, 2014), and were approved by the Italian Ministry of Health. Fifteen to 24 days post-injection, sagittal slices of the rat hippocampus (350 μm thick) were prepared with a Vibratome (Leica VT1200S). Slices were maintained submerged in gassed (95% O_2, 5% CO_2) aCSF containing 123 mM NaCl, 1.25 mM KCl, 1.25 mM KH_2PO4, 1.5 mM $MgCl_2$, 1 mM $CaCl_2$, 25 mM $NaHCO_3$, 2 mM NaPyruvate, and 18 mM glucose (osmolarity adjusted to 300 mOsm). After recovering for 30 min at 37°C and for ≥30 min at room temperature, slices were transferred to a submerged recording chamber and superfused with the same aCSF used for recovery supplemented with 1.5 mM $CaCl_2$ (total Ca^{2+} 2.5 mM). Whole-cell recordings were obtained from pyramidal neurons in the proximal to medial tract of the CA1 region. The intracellular solution contained 110 mM K-gluconate, 22 mM KCl, 5 mM NaCl, 0.5 mM EGTA, 3 mM $MgCl_2$, 4 mM Mg-ATP, 0.5 mM Na_3-GTP, 20 mM K_2-creatine phosphate,

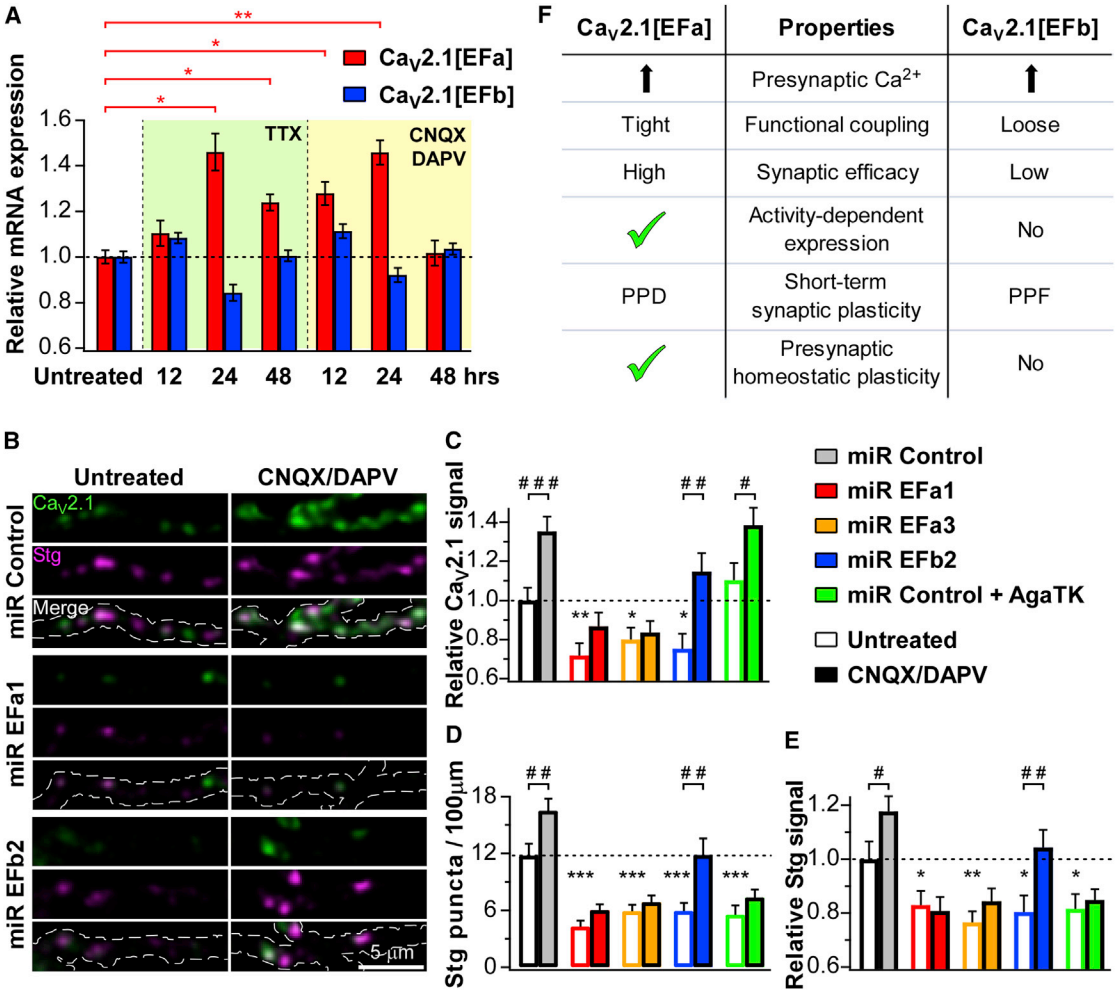

Figure 7. Expression of $Ca_v2.1$[EFa] Is Selectively Regulated by Activity, and It Is Required for Presynaptic Homeostatic Plasticity

(A) Network activity of primary hippocampal cultures was suppressed with either TTX (1 µM) or CNQX (20 µM) and D-APV (100 µM) for the indicated time period. RT-qPCR analysis was performed on RNA isolated at 18 DIV (n = 6 independent experiments). Data are normalized to untreated controls. Chronic activity deprivation with either TTX or CNQX/DAPV increases selectively the mRNA of $Ca_v2.1$[EFa], with the effect being maximal after 24 hr (*p ≤ 0.04, **p = 0.004). (B–E) Effects of $Ca_v2.1$ splice isoform-specific knockdown on synaptotagmin antibody uptake in untreated and silenced cultures. (B) Confocal microscopy images of primary hippocampal axons expressing the indicated microRNAs (miRs) under basal conditions (untreated) and upon activity deprivation with CNQX (20 µM) and D-APV (100 µM) for 24 hr (CNQX/DAPV). $Ca_v2.1$ (green) was detected with an antibody recognizing both splice isoforms; synaptotagmin antibody uptake (Stg, magenta) was carried out at 37°C for 12 min; transfected axons were identified with TdTomato (outline indicated by dashed lines in merge). (C–E) Quantification of experiments as in (B) showing that in untreated cultures (white-filled bars), knockdown of either $Ca_v2.1$[EFa] (miR EFa1 or miR EFa3) or $Ca_v2.1$[EFb] (miR EFb2) reduces the total number of Stg puncta (D), their fluorescence intensity (E), and the fluorescent signal of $Ca_v2.1$ co-localizing with Stg (C), relative to controls (miR control). The number and intensity of Stg puncta is also reduced by pharmacological blockade of $Ca_v2.1$ with ω-agatoxin TK (300 nM; miR control+AgaTK; *p < 0.05, **p < 0.004, and ***p ≤ 0.0003). Chronic treatment with CNQX and D-APV (color-filled bars) increases Stg uptake and $Ca_v2.1$ signal in controls. Both effects are blocked by knockdown of $Ca_v2.1$[EFa] but not by knockdown of $Ca_v2.1$[EFb]. The up-scaling of Stg is also prevented by blocking pharmacologically $Ca_v2.1$ (miR control+AgaTK; n = 40, 40, 38, 36, and 37 fields of view for miR control, miR EFa1, miR EFa3, miR EFb2, and miR control+AgaTK untreated, respectively; n = 40, 38, 39, 38, and 39 fields of view for miR control, miR EFa1, miR EFa3, miR EFb2, and miR control+AgaTK CNQX/DAPV, respectively; #p < 0.05, ##p < 0.01, and ###p = 0.0008). These data suggest that the increase in $Ca_v2.1$ at synapses upon activity deprivation is due largely to $Ca_v2.1$[EFa] and that this splice isoform is selectively required for the expression of presynaptic homeostatic plasticity. Data are presented as mean ± SEM. (F) Summary of the differential properties of $Ca_v2.1$ splice isoforms on synaptic transmission and presynaptic plasticity.
See also Figures S6 and S7.

10 mM HEPES-KOH (pH 7.28, osmolarity adjusted to 290 mOsm). Experiments were performed in the presence of 10 µM bicuculline. EPSCs were evoked with a 473 nm Blue Laser (MBL-III-473 Solid State 1–200 mW; Information Unlimited) coupled via a 20× 0.40 N.A. objective to an optical fiber (250 µm in diameter) positioned directly on CA3 somata. Stimulation strength (1–3 mW at fiber exit) was adjusted with neutral density filters to yield small, but clearly detectable, EPSCs (<30 pA peak amplitude at −70 mV; see Supplemental Experimental Procedures).

Live Imaging

Imaging was performed in rat primary cultures using SyGCaMP3, SyGCaMP6s, or Fluo-4 as a reporter for Ca^{2+} and SypHy as a reporter for vesicle turnover.

SypHy was imaged in aCSF containing 140 mM NaCl, 2.5 mM KCl, 2.2 mM $CaCl_2$, 1.5 mM $MgCl_2$, 13 mM D-glucose, 0.01 mM CNQX, 0.05 mM D-APV, and 12 mM HEPES-NaOH (pH 7.38, osmolarity adjusted to 320 mOsm). Images were captured at 2 Hz with 100 ms integration times using a cooled charge-coupled device (CCD) camera (ORCA-R2; Hamamatsu) and analyzed offline using ImageJ (http://imagej.nih.gov/ij) and the plugin Time Series Analyzer (http://imagej.nih.gov/ij/plugins/time-series.html) using regions of interest (ROIs) 3.2 μm in diameter. The intensity of a twin ROI positioned within 10 μm of the first was used to subtract the local background noise. Signals were quantified as $\Delta F = F - F_0$, where F_0 was measured over a 5 s period prior to stimulation (see Supplemental Experimental Procedures).

Synaptotagmin Antibody Live Uptake

Cultures were treated with CNQX (20 μM) and D-APV (100 μM) 24 hr prior to experiments. N-type Ca^{2+} channels were always blocked with ω-conotoxin GVIA (1 μM) starting 30 min prior to uptake. A subset of coverslips treated also with ω-agatoxin TK (300 nM) for the same time period served as negative control. Neurons were rinsed twice in aCSF containing 140 mM NaCl, 5 mM KCl, 2.2 mM $CaCl_2$, 1.5 mM $MgCl_2$, 15 mM D-glucose, 0.01 mM CNQX, 0.05 mM D-APV, 0.001 mM ω-conotoxin GVIA, and 12 mM HEPES-NaOH, with or without 0.0003 mM ω-agatoxin TK (pH 7.38, osmolarity adjusted to 320 mOsm), before performing the synaptotagmin antibody live uptake in the same aCSF for 12 min at 37°C with a mouse antibody against the luminal domain of synaptotagmin 1 (1:200; catalog no. 105311, Synaptic Systems). After three washes in the same aCSF, neurons were fixed and processed for immunofluorescence, as described in Supplemental Experimental Procedures.

Statistics

Unless otherwise stated, statistical differences were assessed using paired and unpaired two-tailed Student's t test and the one-way ANOVA test followed by the Tukey-Kramer post-test, as required. Analysis of covariance was used for Figures 1E, 3D, and 6E and the Kruskal-Wallis test followed by Dunn's multiple comparison post-test for Figure 1G (Prism 5; GraphPad Software). Unless otherwise stated, average data are expressed as mean + SEM.

SUPPLEMENTAL INFORMATION

Supplemental Information includes Supplemental Experimental Procedures and seven figures and can be found with this article online at http://dx.doi.org/10.1016/j.celrep.2017.06.055.

AUTHOR CONTRIBUTIONS

L.A.C., Y.G., and T.W.S. conceived the project. L.A.C., A.T., Y.G., K.E.V., A.C., and T.W.S. designed research and discussed experiments. L.A.C., A.T., A.C., Y.S.E., and T.N. performed experiments. L.A.C., A.T., A.C., Y.S.E., and K.E.V. analyzed data. L.A.C. wrote the manuscript.

ACKNOWLEDGMENTS

We thank F. Benfenati and A. Dityatev (Istituto Italiano di Tecnologia [IIT]) for support, S.M. Voglmaier (University of California, San Francisco [UCSF]) for SyGCaMP3, and C. Balbi and L. Bassi (IIT) for technical help. This work was supported by IIT and BMRC grant no. 08/1/21/19/557 (Singapore).

Received: April 22, 2017
Revised: June 4, 2017
Accepted: June 21, 2017
Published: July 11, 2017

REFERENCES

Altier, C., Dale, C.S., Kisilevsky, A.E., Chapman, K., Castiglioni, A.J., Matthews, E.A., Evans, R.M., Dickenson, A.H., Lipscombe, D., Vergnolle, N., and Zamponi, G.W. (2007). Differential role of N-type calcium channel splice isoforms in pain. J. Neurosci. *27*, 6363–6373.

Andrade, A., Denome, S., Jiang, Y.Q., Marangoudakis, S., and Lipscombe, D. (2010). Opioid inhibition of N-type Ca^{2+} channels and spinal analgesia couple to alternative splicing. Nat. Neurosci. *13*, 1249–1256.

Bell, T.J., Thaler, C., Castiglioni, A.J., Helton, T.D., and Lipscombe, D. (2004). Cell-specific alternative splicing increases calcium channel current density in the pain pathway. Neuron *41*, 127–138.

Bourinet, E., Soong, T.W., Sutton, K., Slaymaker, S., Mathews, E., Monteil, A., Zamponi, G.W., Nargeot, J., and Snutch, T.P. (1999). Splicing of alpha 1A subunit gene generates phenotypic variants of P- and Q-type calcium channels. Nat. Neurosci. *2*, 407–415.

Cao, Y.Q., and Tsien, R.W. (2010). Different relationship of N- and P/Q-type Ca^{2+} channels to channel-interacting slots in controlling neurotransmission at cultured hippocampal synapses. J. Neurosci. *30*, 4536–4546.

Chaudhuri, D., Chang, S.Y., DeMaria, C.D., Alvania, R.S., Soong, T.W., and Yue, D.T. (2004). Alternative splicing as a molecular switch for Ca^{2+}/calmodulin-dependent facilitation of P/Q-type Ca^{2+} channels. J. Neurosci. *24*, 6334–6342.

Chavez-Noriega, L.E., and Stevens, C.F. (1994). Increased transmitter release at excitatory synapses produced by direct activation of adenylate cyclase in rat hippocampal slices. J. Neurosci. *14*, 310–317.

Davydova, D., Marini, C., King, C., Klueva, J., Bischof, F., Romorini, S., Montenegro-Venegas, C., Heine, M., Schneider, R., Schröder, M.S., et al. (2014). Bassoon specifically controls presynaptic P/Q-type Ca(2+) channels via RIM-binding protein. Neuron *82*, 181–194.

Dreosti, E., Odermatt, B., Dorostkar, M.M., and Lagnado, L. (2009). A genetically encoded reporter of synaptic activity in vivo. Nat. Methods *6*, 883–889.

Eggermann, E., Bucurenciu, I., Goswami, S.P., and Jonas, P. (2012). Nanodomain coupling between Ca^{2+} channels and sensors of exocytosis at fast mammalian synapses. Nat. Rev. Neurosci. *13*, 7–21.

Frank, C.A., Kennedy, M.J., Goold, C.P., Marek, K.W., and Davis, G.W. (2006). Mechanisms underlying the rapid induction and sustained expression of synaptic homeostasis. Neuron *52*, 663–677.

Graves, T.D., Imbrici, P., Kors, E.E., Terwindt, G.M., Eunson, L.H., Frants, R.R., Haan, J., Ferrari, M.D., Goadsby, P.J., Hanna, M.G., et al. (2008). Premature stop codons in a facilitating EF-hand splice variant of CaV2.1 cause episodic ataxia type 2. Neurobiol. Dis. *32*, 10–15.

Gray, A.C., Raingo, J., and Lipscombe, D. (2007). Neuronal calcium channels: splicing for optimal performance. Cell Calcium *42*, 409–417.

Gunaydin, L.A., Yizhar, O., Berndt, A., Sohal, V.S., Deisseroth, K., and Hegemann, P. (2010). Ultrafast optogenetic control. Nat. Neurosci. *13*, 387–392.

Hessler, N.A., Shirke, A.M., and Malinow, R. (1993). The probability of transmitter release at a mammalian central synapse. Nature *366*, 569–572.

Hibino, H., Pironkova, R., Onwumere, O., Vologodskaia, M., Hudspeth, A.J., and Lesage, F. (2002). RIM binding proteins (RBPs) couple Rab3-interacting molecules (RIMs) to voltage-gated Ca(2+) channels. Neuron *34*, 411–423.

Hoppa, M.B., Lana, B., Margas, W., Dolphin, A.C., and Ryan, T.A. (2012). $\alpha 2\delta$ expression sets presynaptic calcium channel abundance and release probability. Nature *486*, 122–125.

Hu, Q., Saegusa, H., Hayashi, Y., and Tanabe, T. (2005). The carboxy-terminal tail region of human Cav2.1 (P/Q-type) channel is not an essential determinant for its subcellular localization in cultured neurones. Genes Cells *10*, 87–96.

Jakawich, S.K., Nasser, H.B., Strong, M.J., McCartney, A.J., Perez, A.S., Rakesh, N., Carruthers, C.J., and Sutton, M.A. (2010). Local presynaptic activity gates homeostatic changes in presynaptic function driven by dendritic BDNF synthesis. Neuron *68*, 1143–1158.

Kaeser, P.S., Deng, L., Wang, Y., Dulubova, I., Liu, X., Rizo, J., and Südhof, T.C. (2011). RIM proteins tether Ca^{2+} channels to presynaptic active zones via a direct PDZ-domain interaction. Cell *144*, 282–295.

Kiyonaka, S., Wakamori, M., Miki, T., Uriu, Y., Nonaka, M., Bito, H., Beedle, A.M., Mori, E., Hara, Y., De Waard, M., et al. (2007). RIM1 confers sustained activity and neurotransmitter vesicle anchoring to presynaptic Ca^{2+} channels. Nat. Neurosci. *10*, 691–701.

Lautermilch, N.J., Few, A.P., Scheuer, T., and Catterall, W.A. (2005). Modulation of CaV2.1 channels by the neuronal calcium-binding protein visinin-like protein-2. J. Neurosci. *25*, 7062–7070.

Lazarevic, V., Schöne, C., Heine, M., Gundelfinger, E.D., and Fejtova, A. (2011). Extensive remodeling of the presynaptic cytomatrix upon homeostatic adaptation to network activity silencing. J. Neurosci. *31*, 10189–10200.

Lee, A., Westenbroek, R.E., Haeseleer, F., Palczewski, K., Scheuer, T., and Catterall, W.A. (2002). Differential modulation of Ca(v)2.1 channels by calmodulin and Ca^{2+}-binding protein 1. Nat. Neurosci. *5*, 210–217.

Lipscombe, D., Allen, S.E., and Toro, C.P. (2013). Control of neuronal voltage-gated calcium ion channels from RNA to protein. Trends Neurosci. *36*, 598–609.

Mantuano, E., Romano, S., Veneziano, L., Gellera, C., Castellotti, B., Caimi, S., Testa, D., Estienne, M., Zorzi, G., Bugiani, M., et al. (2010). Identification of novel and recurrent CACNA1A gene mutations in fifteen patients with episodic ataxia type 2. J. Neurol. Sci. *291*, 30–36.

Maximov, A., Südhof, T.C., and Bezprozvanny, I. (1999). Association of neuronal calcium channels with modular adaptor proteins. J. Biol. Chem. *274*, 24453–24456.

Mochida, S., Sheng, Z.H., Baker, C., Kobayashi, H., and Catterall, W.A. (1996). Inhibition of neurotransmission by peptides containing the synaptic protein interaction site of N-type Ca^{2+} channels. Neuron *17*, 781–788.

Pragnell, M., De Waard, M., Mori, Y., Tanabe, T., Snutch, T.P., and Campbell, K.P. (1994). Calcium channel beta-subunit binds to a conserved motif in the I-II cytoplasmic linker of the alpha 1-subunit. Nature *368*, 67–70.

Raj, B., and Blencowe, B.J. (2015). Alternative splicing in the mammalian nervous system: recent insights into mechanisms and functional roles. Neuron *87*, 14–27.

Reid, C.A., Bekkers, J.M., and Clements, J.D. (1998). N- and P/Q-type Ca^{2+} channels mediate transmitter release with a similar cooperativity at rat hippocampal autapses. J. Neurosci. *18*, 2849–2855.

Rettig, J., Sheng, Z.H., Kim, D.K., Hodson, C.D., Snutch, T.P., and Catterall, W.A. (1996). Isoform-specific interaction of the alpha1A subunits of brain Ca^{2+} channels with the presynaptic proteins syntaxin and SNAP-25. Proc. Natl. Acad. Sci. U S A *93*, 7363–7368.

Rosenmund, C., Clements, J.D., and Westbrook, G.L. (1993). Nonuniform probability of glutamate release at a hippocampal synapse. Science *262*, 754–757.

Schneider, R., Hosy, E., Kohl, J., Klueva, J., Choquet, D., Thomas, U., Voigt, A., and Heine, M. (2015). Mobility of calcium channels in the presynaptic membrane. Neuron *86*, 672–679.

Scholz, K.P., and Miller, R.J. (1995). Developmental changes in presynaptic calcium channels coupled to glutamate release in cultured rat hippocampal neurons. J. Neurosci. *15*, 4612–4617.

Sheng, Z.H., Rettig, J., Takahashi, M., and Catterall, W.A. (1994). Identification of a syntaxin-binding site on N-type calcium channels. Neuron *13*, 1303–1313.

Simms, B.A., and Zamponi, G.W. (2014). Neuronal voltage-gated calcium channels: structure, function, and dysfunction. Neuron *82*, 24–45.

Soong, T.W., DeMaria, C.D., Alvania, R.S., Zweifel, L.S., Liang, M.C., Mittman, S., Agnew, W.S., and Yue, D.T. (2002). Systematic identification of splice variants in human P/Q-type channel alpha1(2.1) subunits: implications for current density and Ca^{2+}-dependent inactivation. J. Neurosci. *22*, 10142–10152.

Vigues, S., Gastaldi, M., Massacrier, A., Cau, P., and Valmier, J. (2002). The alpha(1A) subunits of rat brain calcium channels are developmentally regulated by alternative RNA splicing. Neuroscience *113*, 509–517.

Vyleta, N.P., and Jonas, P. (2014). Loose coupling between Ca^{2+} channels and release sensors at a plastic hippocampal synapse. Science *343*, 665–670.

Wu, L.G., Westenbroek, R.E., Borst, J.G., Catterall, W.A., and Sakmann, B. (1999). Calcium channel types with distinct presynaptic localization couple differentially to transmitter release in single calyx-type synapses. J. Neurosci. *19*, 726–736.

Zhao, C., Dreosti, E., and Lagnado, L. (2011). Homeostatic synaptic plasticity through changes in presynaptic calcium influx. J. Neurosci. *31*, 7492–7496.

Cell Reports, Volume *20*

Supplemental Information

Alternative Splicing of P/Q-Type Ca^{2+} Channels Shapes Presynaptic Plasticity

Agnes Thalhammer, Andrea Contestabile, Yaroslav S. Ermolyuk, Teclise Ng, Kirill E. Volynski, Tuck Wah Soong, Yukiko Goda, and Lorenzo A. Cingolani

This file includes:

SUPPLEMENTAL FIGURES

SUPPLEMENTAL EXPERIMENTAL PROCEDURES

SUPPLEMENTAL REFERENCES

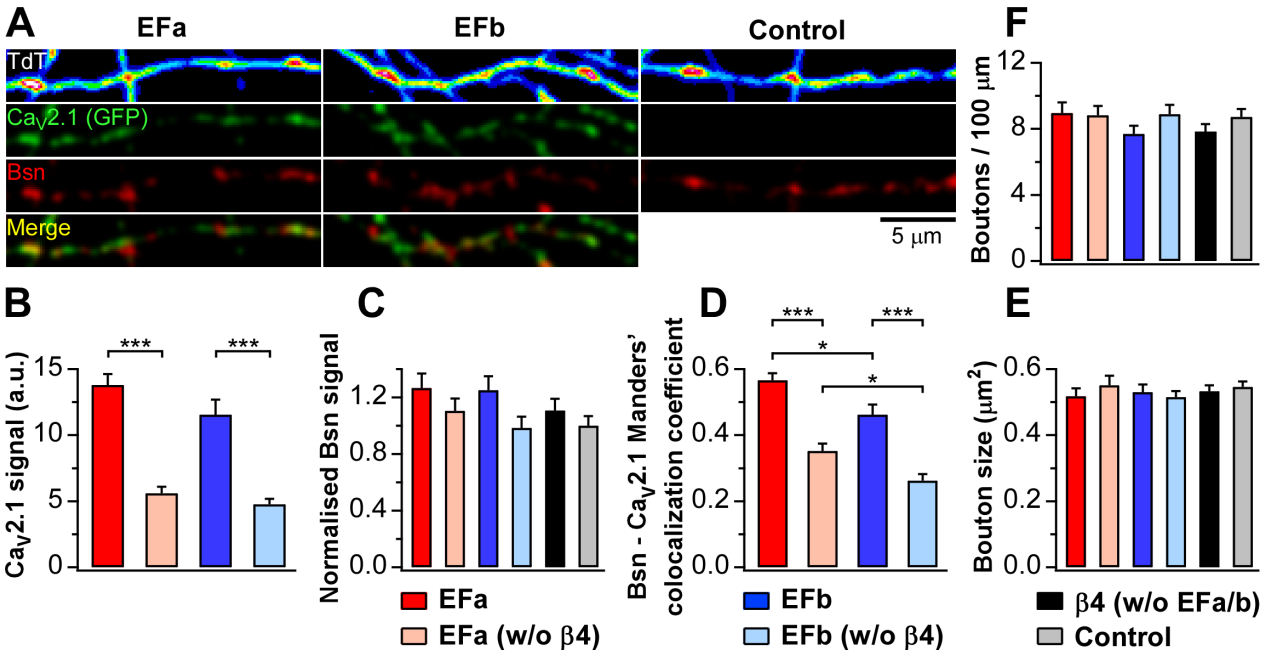

Figure S1. **Exogenous $Ca_v2.1$[EFa] and $Ca_v2.1$[EFb] are targeted to axons and presynaptic boutons.** Related to figures 1, 2 and 3. **(A)** Confocal microscopy images of primary hippocampal axons expressing $Ca_v2.1$[EFa] (EFa; left panels) or $Ca_v2.1$[EFb] (EFb; middle panels) tagged with EGFP at the N-terminus, together with the auxiliary subunit β4 and TdTomato. In Control (right panel), only TdTomato was expressed. Bassoon (Bsn) and TdTomato (TdT) were used as presynaptic and morphological markers, respectively. Both splice isoforms are targeted to axons and presynaptic boutons. **(B)** Quantification of $Ca_v2.1$[EFa] and $Ca_v2.1$[EFb] expression levels for experiments as in (A), showing the requirement of the auxiliary subunit β4 for effective expression and axonal targeting of $Ca_v2.1$[EFa] and $Ca_v2.1$[EFb]. **(C)** Quantification of the effects of exogenous constructs on bassoon expression level. Data are normalized to controls. **(D)** The Mander's co-localization coefficient for bassoon with $Ca_v2.1$ in the four experimental conditions considered. The co-localization of bassoon with $Ca_v2.1$[EFa] is ~20% higher than that with $Ca_v2.1$[EFb]. Co-expression of β4 increases the Mander's coefficient for both splice isoforms without affecting their relative differences (n = 40, 40, 41, 40, 44 and 42 fields of view for EFa, EFa (w/o β4), EFb, EFb (w/o β4), β4 (w/o EFa/b) and Control, respectively; *$p<0.05$ and ***$p<0.001$). **(E, F)** Quantification of the effects of exogenous constructs on bouton size (E) and number (F). Data are presented as mean±SEM.

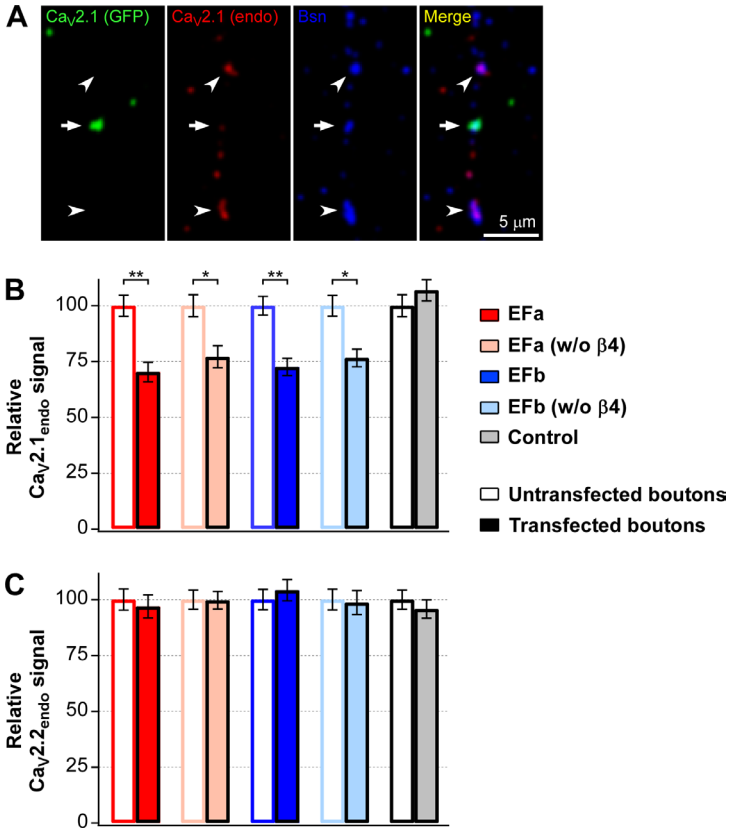

Figure S2. Exogenous $Ca_v2.1$[EFa] and $Ca_v2.1$[EFb] partially replace endogenous $Ca_v2.1$ channels. Related to figures 1, 2 and 3. **(A)** Primary hippocampal neurons were sparsely transfected with human $Ca_v2.1$[EFb] tagged with EGFP at the N-terminus and the auxiliary subunit β4. Confocal microscopy was used to co-label exogenous human $Ca_v2.1$ channels, via the EGFP tag (green), endogenous $Ca_v2.1$ channels (red), using an antibody specific for rodent $Ca_v2.1$ channels (Schneider et al., 2015), and the presynaptic marker bassoon (Bsn, blue). The expression level of endogenous $Ca_v2.1$ channels is reduced in transfected boutons (arrows) as compared to nearby untransfected boutons (arrow heads). **(B)** Quantification for experiment as in (A). In Control only EGFP was expressed. Expression of exogenous $Ca_v2.1$[EFa] or $Ca_v2.1$[EFb], with or without co-expression of the auxiliary subunit β4, reduces the expression level of endogenous P/Q-type $Ca_v2.1$ channels (n = 100 boutons for each condition; *p≤0.04, **p≤0.007). **(C)** As in (B) but for endogenous N-type $Ca_v2.2$ channels. Expression of exogenous $Ca_v2.1$ splice isoforms does not significantly affect the expression level of endogenous $Ca_v2.2$ channels (n = 100 boutons for each condition). Data are presented as mean±SEM.

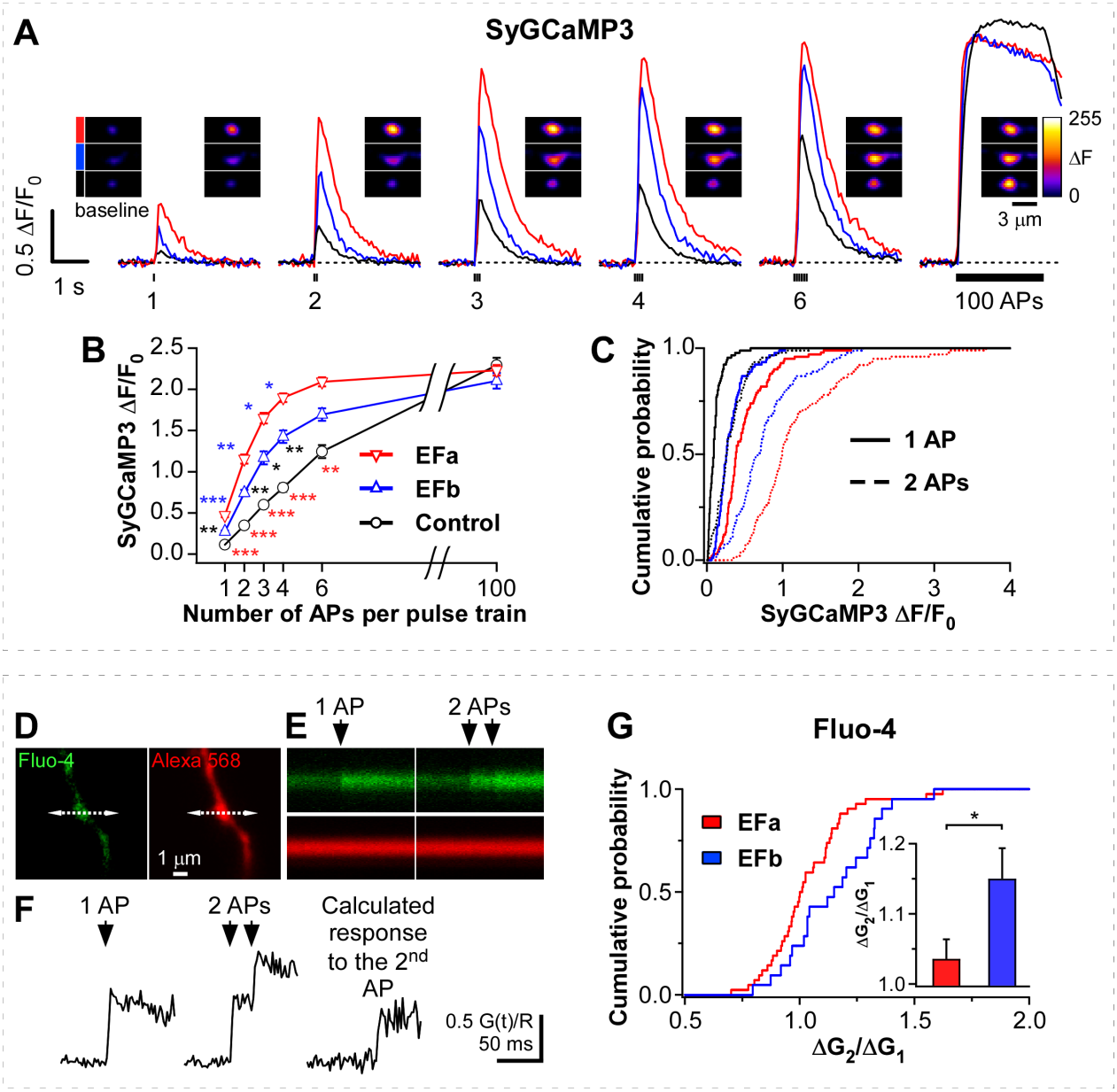

Figure S3. **Exogenous $Ca_v2.1$[EFa] and $Ca_v2.1$[EFb] boost presynaptic Ca^{2+} signals.** Related to figures 1, 2 and 3. **(A-C)** Imaging presynaptic Ca^{2+} transients with SyGCaMP3 in primary hippocampal cultures. **(A)** SyGCaMP3 responses from representative experiments. Traces show averages of 31, 15 and 18 boutons from individual fields of view for $Ca_v2.1$[EFa] (red), $Ca_v2.1$[EFb] (blue) and Control (black; boutons without expression of exogenous $Ca_v2.1$ channels) in response to the indicated number of APs delivered at 40Hz. Inset, individual boutons for the three conditions. **(B)** Average peak amplitude of SyGCaMP3 for experiments as in (A) (n=7, 8 and 8 independent experiments for $Ca_v2.1$[EFa], $Ca_v2.1$[EFb] and Control, respectively; *p<0.05, **p<0.01 and ***p<0.001). **(C)** Cumulative distribution of individual boutons in response to one (continuous lines) and two (dotted lines) APs for $Ca_v2.1$[EFa] (n=100), $Ca_v2.1$[EFb] (n=91) and Control (n=91). $Ca_v2.1$[EFa] is more efficient than $Ca_v2.1$[EFb] in increasing SyGCaMP3 signals. **(D-F)** Typical experiment for imaging presynaptic Ca^{2+} dynamics with Fluo-4 in primary hippocampal cultures. **(D)** Images of a presynaptic bouton and axonal fragment of a $Ca_v2.1$[EFa] neuron (left, Fluo-4 channel; right, Alexa 568 channel; dotted lines indicate positions of the line-scan for recording fast AP-evoked Ca^{2+} dynamics). **(E)** Fluorescence responses to single (left) and paired (25 ms interval; right) APs in the bouton from (D). Top, Fluo-4 channel; bottom, Alexa 568 channel. Images are averages of five sweeps. **(F)** Fluo-4 responses to one (left) and two APs (middle) normalized to Alexa568 fluorescence (G(t)/R) from (E). Right, digitally calculated response to the second AP. **(G)** Ratio of the fluorescence responses between the second and first AP ($\Delta G_2/\Delta G_1$) for individual boutons (n = 42 and 21 for $Ca_v2.1$[EFa] and $Ca_v2.1$[EFb], respectively) for experiments as in (D-F). Inset, bar graph summary of the same data. $Ca_v2.1$[EFb] induces a small paired-pulse facilitation of presynaptic Ca^{2+} signals (*p=0.03). Data are presented as mean±SEM.

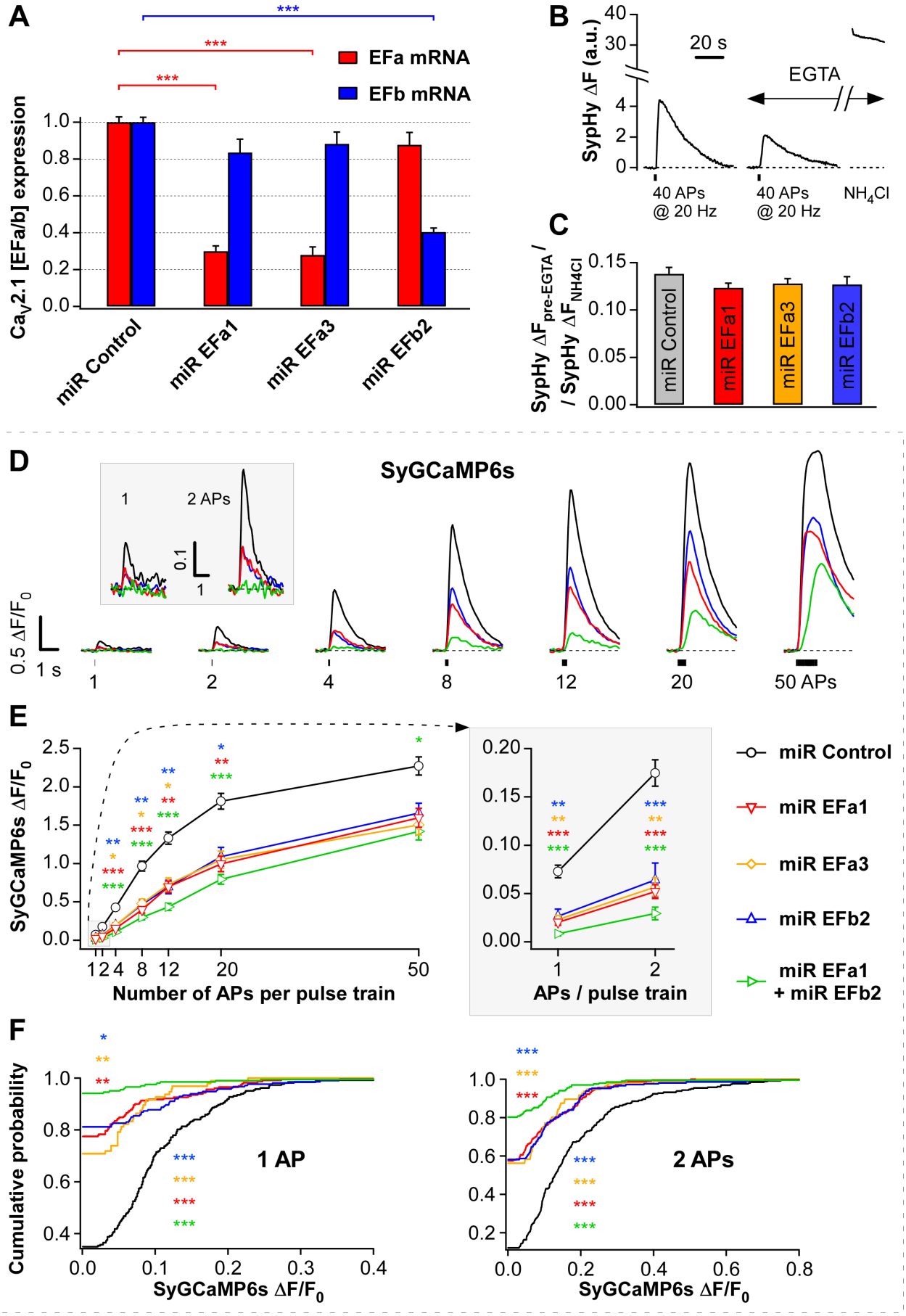
A
***
***
***
EFa mRNA
EFb mRNA
Cav2.1 [EFa/b] expression
1.0
0.8
0.6
0.4
0.2
0.0
miR Control
miR EFa1
miR EFa3
miR EFb2
B
SypHy ΔF (a.u.)
40
30
4
2
0
20 s
EGTA
40 APs
@ 20 Hz
40 APs
@ 20 Hz
NH4Cl
C
SypHy ΔFpre-EGTA / SypHy ΔFNH4Cl
0.15
0.10
0.05
0.00
miR Control
miR EFa1
miR EFa3
miR EFb2
D
SyGCaMP6s
1
2 APs
0.1
1
0.5 ΔF/F0
1 s
1
2
4
8
12
20
50 APs
E
SyGCaMP6s ΔF/F0
2.5
2.0
1.5
1.0
0.5
0.0
1 2 4 8 12 20 50
Number of APs per pulse train
0.20
0.15
0.10
0.05
0.00
1
2
APs / pulse train
miR Control
miR EFa1
miR EFa3
miR EFb2
miR EFa1
+ miR EFb2
F
Cumulative probability
1.0
0.8
0.6
0.4
1 AP
0.0
0.1
0.2
0.3
0.4
SyGCaMP6s ΔF/F0
2 APs
0.0
0.2
0.4
0.6
0.8
SyGCaMP6s ΔF/F0

Figure S4. **Further characterization of the knockdown of $Ca_v2.1$[EFa] and $Ca_v2.1$[EFb].** Related to figures 4, 5 and 6. **(A)** Evaluation of the knockdown efficiency and selectivity of isoform-specific microRNAs (miRs) for $Ca_v2.1$[EFa] and $Ca_v2.1$[EFb]. Isoform-specific RT-qPCR analysis on RNA isolated from 17-18 DIV primary cultures infected at 6 DIV with adeno-associated viruses (AAVs) expressing miRs targeting either $Ca_v2.1$[EFa] (miR EFa1 and miR EFa3) or $Ca_v2.1$[EFb] (miR EFb2). Data are normalized to the negative control (miR Control). miR EFa1 and miR EFa3 significantly reduce mRNA of $Ca_v2.1$[EFa] (by ~70%; n = 8 and 7 cultures) but not that of $Ca_v2.1$[EFb], whilst miR EFb significantly reduces mRNA of $Ca_v2.1$[EFb] (by ~60%; n = 4 cultures; ***$p<0.001$) but not that of $Ca_v2.1$[EFa]. For detailed information on the knockdown strategy refer to supplemental experimental procedures. **(B)** Typical experiment for imaging vesicle release with SypHy in primary hippocampal cultures following transfection with isoform-specific miRs for $Ca_v2.1$[EFa] and $Ca_v2.1$[EFb]. SypHy responses for miR Control to 40 APs delivered at 20 Hz before and after EGTA-AM application (200 μM, loaded for 90 s, followed by 10 min wash), and following rapid alkalization of the entire vesicle pool with NH_4Cl (50 mM), as indicated. **(C)** Summary of experiments as in (B) (n=10, 13, 12 and 11 independent experiments for miR Control, miR EFa1, miR EFa3 and miR EFb2, respectively). Knockdown of either $Ca_v2.1$[EFa] or $Ca_v2.1$[EFb] has no effect on the pre-EGTA responses normalized to the total vesicle pool size at each bouton. **(D-F)** Imaging presynaptic Ca^{2+} transients with SyGCaMP6s in primary hippocampal cultures. Presynaptic Ca^{2+} transients are largely reduced by knockdown of either $Ca_v2.1$[EFa] or $Ca_v2.1$[EFb], and severely compromised when both splice isoforms are targeted. SyGCaMP6s recordings were performed in the presence of ω-conotoxin GVIA (1 μM) to block N-type Ca^{2+} channels and measure the contribution of P/Q-type $Ca_v2.1$[EFa] and $Ca_v2.1$[EFb] isoforms to presynaptic Ca^{2+} in relative isolation (see supplemental methods). **(D)** SyGCaMP6s responses from representative experiments. Traces are averages of 17, 20, 19 and 12 boutons from individual fields of view for miR Control (black), miR EFa1 (red), miR EFb2 (blue) and miR EFa1 + miR EFb2 (green) in response to the indicated number of APs delivered at 40 Hz. Inset, higher magnification for one and two APs. **(E)** Average peak amplitude of SyGCaMP6s for experiments as in (D) (n=18, 14, 9, 16 and 14 independent experiments for miR Control, miR EFa1, miR EFa3 (orange), miR EFb2 and miR EFa1 + miR EFb2, respectively; *$p<0.05$, **$p<0.01$ and ***$p<0.001$. Inset, higher magnification for one and two APs. **(F)** Cumulative distribution of $\Delta F/F_0$ for individual boutons in response to one (left) and two (right) APs (n=263, 231, 96, 213 and 203 boutons for miR Control, miR EFa1, miR EFa3, miR EFb2 and miR EFa1+EFb2, respectively). Data are presented as mean±SEM.

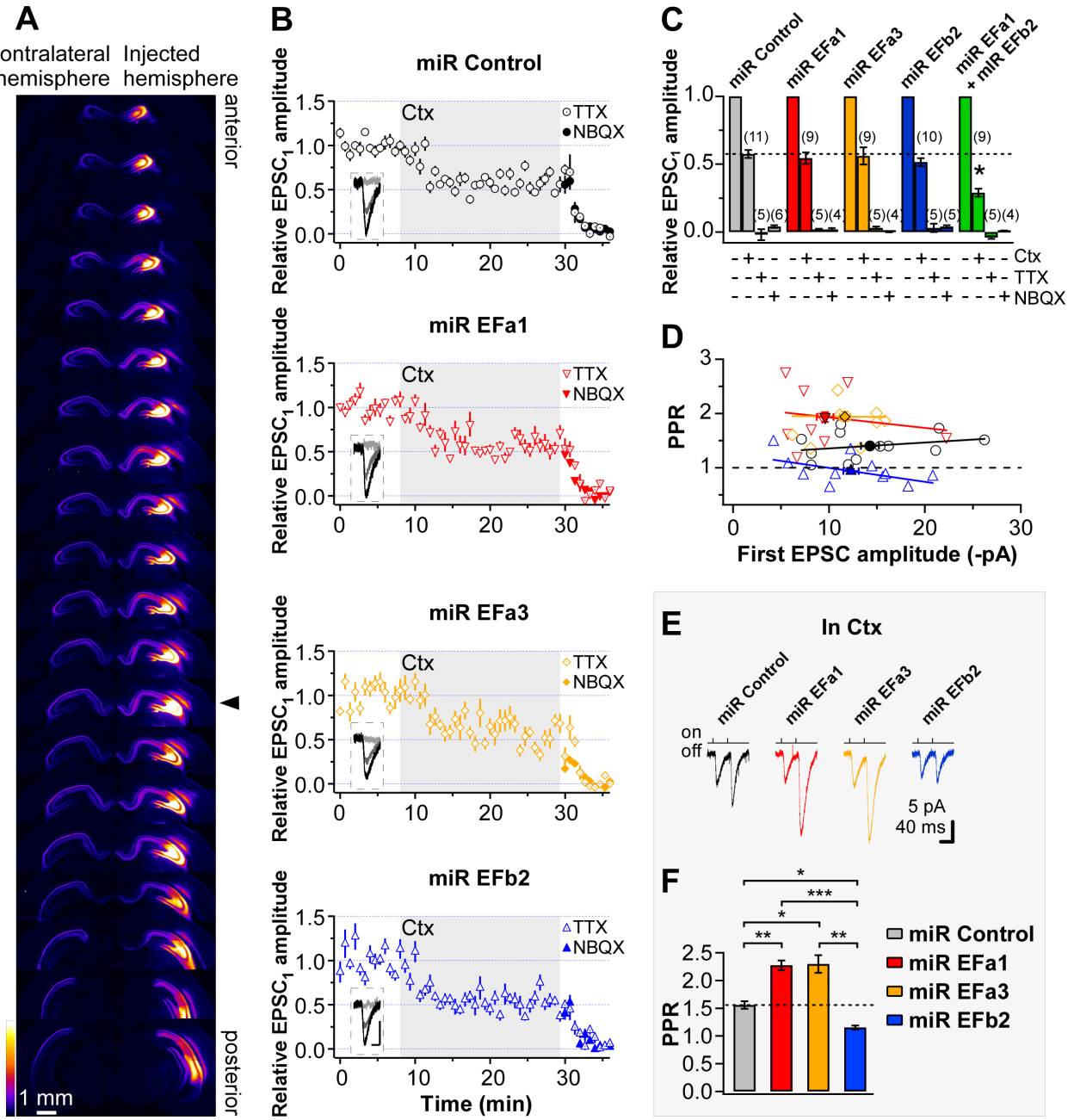

Figure S5. **Further optogenetic characterization in acute brain slices of the *in vivo* knockdown of $Ca_V2.1$[EFa] and $Ca_V2.1$[EFb].** Related to figure 6. **(A)** Serial coronal sections of rat brain aligned along the anterior-posterior axis. AAV, expressing miR Control and the ultrafast channelrhodopsin ChETA fused to TdTomato, was stereotactically injected into the CA3 region of the right hippocampus at the indicated location (arrowhead). TdTomato fluorescence is visible in the CA3 region and in CA3 ipsi- and contra-lateral axonal projections along the anterior-posterior axis. Optogenetic experiments were done with bilateral injections. **(B, C)** Acute application of ω-conotoxin GVIA (1 µM; Ctx) induces a ~42% reduction of the amplitude of optogenetically evoked EPSCs under control conditions (miR Control), similarly to the previously reported effect of Ctx on electrically evoked EPSCs at these synapses (Reid et al., 1998; Scheuber et al., 2004; Scholz and Miller, 1995; Wu and Saggau, 1994). miR EFa1, miR EFa3 and miR EFb2 do not significantly change this percentage, arguing against a compensatory up-regulation of N-type Ca^{2+} channels upon knockdown of one P/Q-type Ca^{2+} channel splice isoform. When both isoforms are knocked down (miR EFa1 + miR EFb2), the Ctx-dependent reduction of EPSCs is significantly larger than in control conditions (~71%; *p<0.05 relative to miR Control; green scale bars in (C)). Optogenetically evoked EPSCs are completely blocked by TTX or NBQX, indicating that they are AP-dependent and mediated by AMPARs. Insets in (B), representative EPSC traces under basal conditions (Black), after Ctx (dark grey) and TTX (in miR EFa1 and miR EFb2) or NBQX (in miR Control and miR EFa3) application (light gray); scale bars 5 pA and 20 ms. In (C), numbers of recorded cells are indicated in brackets; dashed line refers to the amplitude of EPSCs with Ctx in the miR Control group. **(D)** PPR vs. amplitude of first EPSC during baseline, showing that the differences in PPR are not

secondary to differences in the amplitude of the first EPSC. Lines are linear regression fits. Open symbols represent individual recordings, filled symbols population averages. Stimulation strength was adjusted to yield small EPSCs (<30 pA). (**E, F**) As in (D, E) of figure 6 but after application of Ctx. The increase in PPR with miR EFa1 and miR EFa3 and its decrease with miR EFb2, relative to miR Control, are maintained after blockade of N-type Ca^{2+} channels (*p<0.05; **p<0.005; ***p<0.0001), suggesting that the differences in PPR result from a shift in $Ca_v2.1$ splice isoform composition. Data are presented as mean±SEM.

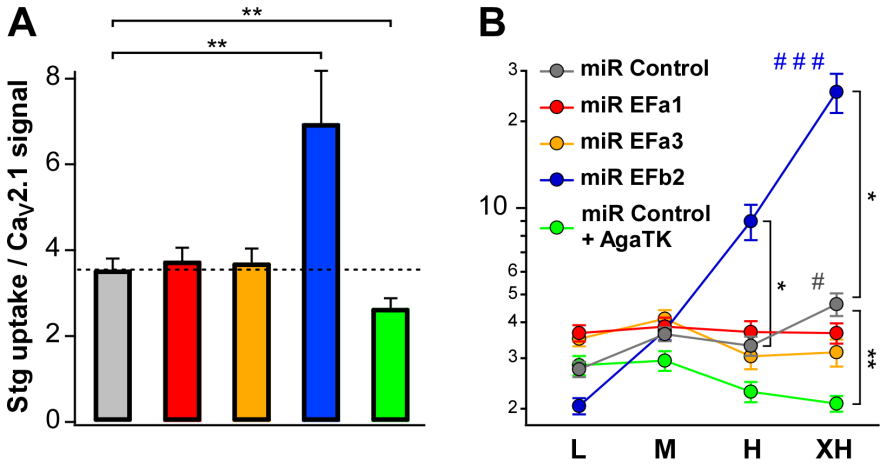

Figure S6. **Relationship between synaptotagmin uptake and $Ca_v2.1$ expression at individual boutons.** Related to figure 7. **(A)** The ratio between synaptotagmin (Stg) uptake level and $Ca_v2.1$ fluorescence signal at individual boutons was taken as measure of presynaptic efficacy of $Ca_v2.1$. Relative to controls (miR Control), synaptic efficacy is largely increased by knockdown of $Ca_v2.1$[EFb] (miR EFb2), unchanged by knockdown of $Ca_v2.1$[EFa] (miR EFa1 and miR EFa3) and reduced by pharmacological blockade of $Ca_v2.1$ channels with ω-agatoxin TK (300 nM; miR Control + AgaTK; **p≤0.009; n = 497, 194, 248, 244 and 232 boutons for miR Control, miR EFa1, miR EFa3, miR EFb2 and miR Control + AgaTK, respectively). (**B**) Boutons were divided into four groups of increasing Stg fluorescent signal (L = low activity, M = medium activity, H = high activity, XH = extra high activity, corresponding to a Stg fluorescent signal of 0-10, 10-20, 20-30 and >30 a.u., respectively), and the average of the ratio between Stg uptake level and $Ca_v2.1$ signal at individual boutons was plotted for each group. In control conditions (miR Control), presynaptic efficacy of $Ca_v2.1$ is moderately higher in more active boutons (# p=0.03). Knockdown of $Ca_v2.1$[EFb] largely increases this correlation (miR EFb2; ### p<0.0001), whereas knockdown of $Ca_v2.1$[EFa] (miR EFa1 and miR EFa3) or pharmacological blockade of $Ca_v2.1$ with ω-agatoxin TK (300 nM; miR Control + AgaTK) abolishes it. Statistical analyses within each of the four groups of increasing activity levels reveal that synaptic efficacy is higher for miR EFb2 in the H and XH groups (*p≤0.03), and smaller for miR Control + AgaTK in the XH group (**p=0.005), relative to miR Control. Same data set as in figure 7B-E. Data are presented as mean±SEM. The relationship between Stg uptake and $Ca_v2.1$ expression at individual boutons in the presence of $Ca_v2.1$ isoform-specific miRs suggests that (i) endogenous $Ca_v2.1$[EFa] (miR EFb2 condition) is overall more efficient than endogenous $Ca_v2.1$[EFb] (miR EFa1 and miR EFa3 conditions) in supporting Stg uptake and that (ii) the efficiency of endogenous $Ca_v2.1$[EFa] is higher at more active boutons, while that of $Ca_v2.1$[EFb] is independent of the activity level of the boutons.

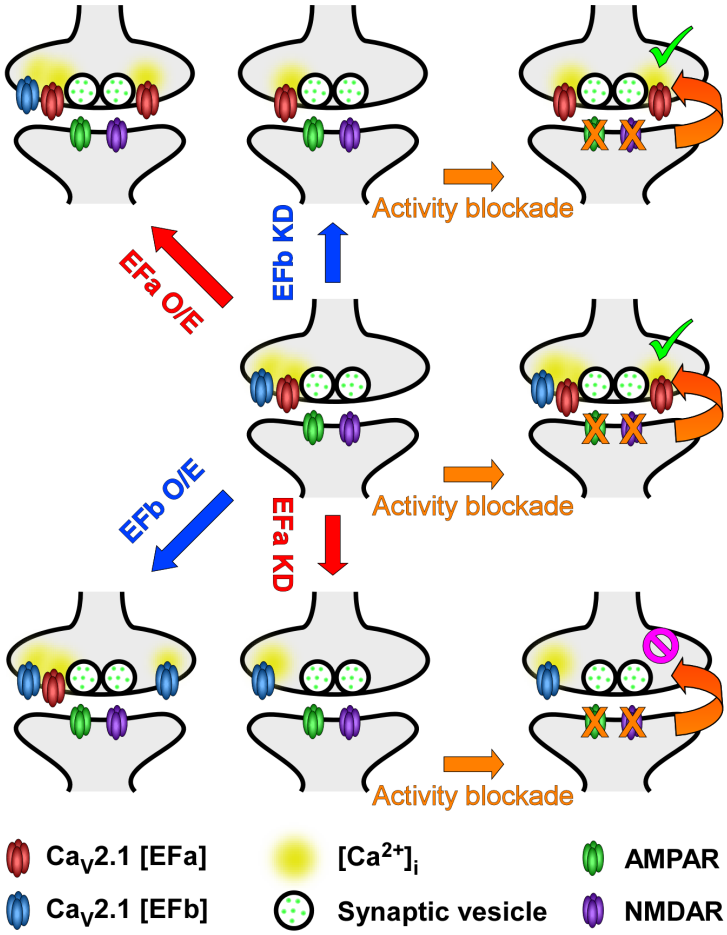

Figure S7. **Working model for $Ca_v2.1$[EFa] and $Ca_v2.1$[EFb] configuration at hippocampal synapses.** Related to all figures. Over-expression of $Ca_v2.1$[EFa] (top left) favors tight coupling between $Ca_v2.1$ channels and synaptic vesicles at most synapses (figure 3), resulting in high P_r (figure 1G and 2) and PPD (figure 1D-F). Over-expression of $Ca_v2.1$[EFb] (bottom left) favors loose coupling at many synapses (figure 3), thus promoting lower P_r (figure 1G and 2) and PPF (figure 1D-F). Knockdown of $Ca_v2.1$[EFb] (top center) leaves in place $Ca_v2.1$[EFa] channels, which display high synaptic efficacy (figure S6) and are less sensitive to EGTA (figure 5); this results in decreased PPR (figure 6). In top right, blockade of postsynaptic AMPA and NMDA receptors activates retrograde signals that lead to presynaptic homeostatic plasticity, involving an increase in vesicle number (not depicted; (Thalhammer and Cingolani, 2014)) and insertion of $Ca_v2.1$[EFa] channels (figure 7B-E), as for naïve boutons (middle left; figure 7B-E). Knockdown of $Ca_v2.1$[EFa] (bottom center) leaves in place $Ca_v2.1$[EFb] channels, which display low synaptic efficacy (figure S6) and are more sensitive to EGTA (figure 5); this results in increased PPR (figure 6). In bottom right, blockade of postsynaptic AMPA and NMDA receptors fails to induce presynaptic homeostatic plasticity because $Ca_v2.1$[EFa] channels for insertion are lacking (figure 7B-E). As for previously proposed models of P/Q-type and N-type Ca^{2+} channels (Cao et al., 2004; Cao and Tsien, 2010), this model assumes that there are P/Q-type channel isoform-specific slots in the presynaptic membrane, with $Ca_v2.1$[EFa] and $Ca_v2.1$[EFb] channels not interchangeable. Drawing is not to scale; numbers of channels and vesicles are not intended to be quantitative.

Supplemental Experimental Procedures

DNA constructs

For experiments in primary cultures, we used human $Ca_v2.1$[Δ10A (+G), 16+/17+, Δ17A (-VEA), +31* (+NP), 37a (EFa), 43+/44+, Δ47] and $Ca_v2.1$[Δ10A (+G), 16+/17+, Δ17A (-VEA), +31* (+NP), 37b (EFb), 43+/44+, Δ47], referred to as $Ca_v2.1$[EFa] and $Ca_v2.1$[EFb], respectively (Chaudhuri et al., 2004) (**figure 1B**). For testing microRNA (miR) efficiency in cell lines, we used rat $Ca_v2.1$[EFa] and $Ca_v2.1$[EFb] (Bourinet et al., 1999). In both cases, we co-transfected the Ca^{2+} channel auxiliary subunit β4 because it favors surface delivery of primary α_{1A} subunits without affecting morphology and number of presynaptic boutons, Ca^{2+} transients or synaptic transmission *per se* (**figure S1B-F** and (Hoppa et al., 2012; Qian and Noebels, 2000).

SyGCaMP3, in which GCaMP3 is fused to the cytoplasmic C-terminus of the synaptic vesicle protein synaptophysin, was kindly provided by Dr. Susan Voglmaier (Li et al., 2011; Niwa et al., 1991). SyGCaMP6s was cloned by swapping GCaMP3 with GCaMP6s (#40753, Addgene) (Chen et al., 2013). SyGCaMP constructs localize to synaptic vesicles, thus sampling Ca^{2+} specifically at presynaptic terminals (Dreosti et al., 2009; Li et al., 2011).

The constructs for adeno-associated virus (AAV) production (Syn-ChETA-TdT-miR-X; **figure 6A**) were derived from pAAV-Ef1a-FAS-ChETA-TdTomato-WPRE-pA (#37089, Addgene) (Saunders et al., 2012) by exchanging the Ef-1a promoter with the short human Synapsin promoter and by cloning the miR cassette from pcDNA6.2-GW/EmGFP-miR vector (K4936-00, Invitrogen) between the stop codon of ChETA-TdTomato and WPRE using the NheI and EcoRI sites. For knockdown experiments in culture ChETA was removed from Syn-ChETA-TdT-miR-X to obtain Syn-TdT-miR-X. Constructs were generated by standard cloning strategies and verified by sequencing. All constructs are available upon request.

RNA interference

mRNA target sequences for rat $Ca_v2.1$[EFa] and $Ca_v2.1$[EFb] used to design artificial microRNAs (miRs) for RNA interferences (RNAi) were selected with a dedicated software (BLOCK-iT RNAi Designer; Invitrogen; https:// rnaidesigner.lifetechnologies.com/rnaiexpress/design.do). The miR sequences were cloned into the pcDNA6.2-GW/EmGFP-miR vector using the BLOCK-iT Pol II miR RNAi Expression Vector kit (K4936-00; Invitrogen), according to the manufacturer's instructions, thereby creating an expression cassette consisting of a 5' miR flanking region, a specific miR sequence and a 3' miR flanking region that can be expressed from the 3' UTR of a reporter gene under the control of a RNA polymerase type II promoter. As a negative control (miR Control), we used the pcDNA6.2-GW/EmGFP-miR-neg plasmid from the kit containing a sequence that does not target any known vertebrate gene. Despite the short size (97 bp) and high similarity (61.86% identity at the nucleotide level) between exons 37a and 37b, we could design three miR sequences against rat $Ca_v2.1$[EFa] (miR EFa1: TCCTTATAGTGAATGCGGCCG; miR EFa2: ATGTCCTTATAGTGAATGCGG; miR EFa3: TTGCAAGCAACCCTATGAGGA) and two against rat $Ca_v2.1$[EFb] (miR EFb1: ATACATGTCCGGGTAAGGCAT; miR EFb2: ATCTGATACATGTCCGGGTAA) with predicted high knockdown efficiency. Sequences given are antisense target sequences. Positions (in bp) relative to exons 37a/b are: 1-21 for miR EFa1; 4-24 for miR EFa2; 76-96 for miR EFa3; 8-28 for miR EFb1; 13-33 for miR EFb2. Numbers of mismatches relative to the corresponding sequence on the non-targeted exon are 8, 7, 8, 7 and 9 for miR EFa1, miR EFa2, miR EFa3, miR EFb1 and miR EFb2, respectively.

The knockdown efficiency of the five selected miRs was first evaluated by co-transfecting HEK293 cells with either rat $Ca_v2.1$[EFa] or $Ca_v2.1$[EFb] and one of the five miR vectors. Co-transfection with miR Control was used as negative control. Forty-eight hours after transfection, cells were lysed, and protein content was analyzed by immunoblot with rabbit anti-$Ca_v2.1$ antibody (1:2000; Cat. No. ACC-001, Alomone Labs) and rabbit anti-Actin (1:5000, Sigma). Based on this heterologous expression system, we selected two miRs against $Ca_v2.1$[EFa] (miR EFa1 and miR EFa3), showing 56% and 64% knockdown efficiency, respectively, and one miR against $Ca_v2.1$[EFb] (miR EFb2), showing 42% knockdown efficiency, to be further optimized and tested for efficiency and specificity against endogenous rat $Ca_v2.1$[EFa] and $Ca_v2.1$[EFb] using isoform-specific real time quantitative PCR (following paragraph and **figure S4A**).

Real Time quantitative PCR (RT-qPCR)

Primary rat cultures were infected at 6 DIV with AAVs expressing miR Control, miR EFa1, miR EFa3 or miR EFb2. RNA was extracted at 17-18 DIV with QIAzol reagent and purified on RNeasy spin columns (Qiagen). RNA samples were quantified with a ND1000 Nanodrop spectrophotometer (Thermo Scientific). Reverse transcription was performed with QuantiTect Reverse Transcription Kit (Qiagen). RT-qPCR was performed in triplicate with 10 ng of template cDNA using QuantiTect SYBR green master mix (Qiagen) on a 7900-HT Fast Real-time System (Applied Biosystem), as previously described (Deidda et al., 2015), with the following universal conditions: 5 min at 95 °C, 40 cycles of denaturation at 95 °C for 15 sec, and annealing/extension at 60 °C for 45 sec. Primers were designed with Beacon Designer software (Premier Biosoft) using a BLAST search in order to avoid significant cross homologies regions with other genes. For detecting $Ca_v2.1$[EFa] and $Ca_v2.1$[EFb], we used isoform-specific forward primers (EFa-fwd: 5' CTTAGGCAAGAAATGTCCTCAT 3'; EFb-fwd: 5' GGTCTTGGGAAGAAGTGC 3') and a common reverse primer (EFab-rev: 5' TTGAAGTGAACGGTGTTGTC 3'). The specificity of the primers was

verified in qPCR reactions in which a plasmid containing either rat $Ca_v2.1$[EFa] or rat $Ca_v2.1$[EFb] was used as template. Product specificity and absence of primer dimers was also verified by melting curve analysis. qPCR reaction efficiency for each primer pair was calculated by the standard curve method with a four points serial dilution of cDNA. Calculated qPCR efficiency for each primer set was used for subsequent analysis. To evaluate miR efficiency and selectivity, data were normalized to glyceraldehyde-3-phosphate dehydrogenase (GAPDH; GAPDH-fwd: 5' GGTGCTGAGTATGTCGTGGA 3'; GAPDH-rev: 5' GATGATGACCCTTTTGGC 3') and β-actin (ACTB; ACTB-fwd: 5' CATCACTATCGGCAATGAGC 3'; ACTB-rev: 5' TCATGGATGCCACAGGATT 3') by the multiple internal control gene method with GeNorm algorithm (Vandesompele et al., 2002) available in qBasePlus software (Biogazelle). To evaluate activity-dependent changes in the expression of $Ca_v2.1$[EFa] and $Ca_v2.1$[EFb] (**figure 7A**), data were normalized to tubulin β3 (TUBB3; TUBB3-fwd: 5' GCCTTTGGACACCTATTCAG 3'; TUBB3-rev: 5' TCACATTCTTTCCTCACGAC 3') and peptidylprolyl isomerase A (PPIA; PPIA-fwd: 5' CACTGGGGAGAAAGGATTTG 3'; PPIA-rev 5' CCATTATGGCGTGTGAAGTC 3') because the expression of these two genes displayed no statistically significant changes upon chronic activity deprivation.

In initial experiments, we noticed that the knockdown efficiency of $Ca_v2.1$[EFb] by miR EFb was ~50%. To increase it to values statistically equivalent to the knockdown efficiency of the other two miRs (**figure S4A**), we duplicated the miR EFb2 cassette in the 3'UTR, according to the BLOCK-iT Pol II miR RNAi Expression Vector kit's instructions, and prepared new constructs containing a double miR EFb2 cassette to be used in all subsequent tests and experiments (**figures 4-7 and S4-S6**).

For the absolute determination of $Ca_v2.1$[EFa] and $Ca_v2.1$[EFb] transcripts, standard curves prepared with serial dilutions of $Ca_v2.1$[EFa]- and $Ca_v2.1$[EFb]-containing plasmids were run in parallel to the experimental samples. RNA extracted from the CA1-CA3 region of the rat hippocampus (P40) yielded 7942±203 copy number/ng RNA (42.9±0.8%) and 10643±320 copy number/ng RNA (57.1±0.8%) for $Ca_v2.1$[EFa] and $Ca_v2.1$[EFb], respectively (n = 5 hippocampi).

AAV production and stereotactic injections

AAV1/2 expressing ChETA-TdT-miR-EFa1, ChETA-TdT-miR-EFa3, ChETA-TdT-miR-EFb2-miR-EFb2 and ChETA-TdT-miR-Control were generated as previously described (McClure et al., 2011). Briefly, HEK293T cells were co-transfected with the required AAV vector together with the plasmids pRV1, pH21 and pFdelta6 using a Ca^{2+} phosphate method. Forty-eight hrs post transfection, cells were harvested and lysed, and viruses purified over heparin columns (Ge HealthCare Life science).

Stereotactic injections were performed in P18 rats, with coordinates for CA3 of (A-P/M-L/D-V from Bregma) −2.6/± 2.9/−2.9. Expression and localization of AAVs was confirmed by TdTomato fluorescence (**figure 6B** and **S5A**).

Electrophysiology in primary cultures

Low density rat primary hippocampal cultures were grown on a glial feeder layer as previously described (Cingolani and Goda, 2008), transfected with $Ca_v2.1$[EFa] or $Ca_v2.1$[EFb] together with the auxiliary subunit β4 (1:1 DNA ratio) 2-5 days prior to experiments using a Ca^{2+} phosphate method (Cingolani et al., 2008) and recorded at 12-15 days in vitro (DIV). Whole-cell paired-recordings were performed at room temperature from a transfected and a nearby untransfected pyramidal neuron. For the data reported in **figure 1**, in the case of $Ca_v2.1$[EFa], out of 16 connected pairs, eight expressed $Ca_v2.1$[EFa] in the presynaptic neuron, five in the postsynaptic one, and three displayed double connectivity; in the case of $Ca_v2.1$[EFb], out of 18 connected pairs, 10 expressed $Ca_v2.1$[EFb] in the presynaptic neuron, seven in the postsynaptic one, and one displayed double connectivity (**figure 1C**). A pair was considered not connected in one direction if no response was observed after ≥10 stimuli. Pairs displaying polysynaptic connectivity were discarded. AMPAR-mediated excitatory postsynaptic currents (EPSCs) were scored with a detection threshold set at two SD of the background noise over time windows of 0-8 and 8-658 ms following the end of the presynaptic Na^+ spike for synchronous and asynchronous release, respectively.

Sister cultures were used for the two splice isoforms, and experiments were performed in parallel on at least three independent preparations. During recordings, neurons were continuously perfused with aCSF containing (in mM): 140 NaCl, 2.5 KCl, 2.2 $CaCl_2$, 2.3 $MgCl_2$, 10 D-glucose, 10 HEPES-NaOH (pH 7.38; osmolarity adjusted to 290 mOsm). A $GABA_A$ receptor blocker (100 μM picrotoxin) was routinely included in the aCSF. For EGTA-AM experiments, $CaCl_2$ was raised to 2.5 mM and $MgCl_2$ lowered to 1.5 mM in order to increase P_r and favor EPSC detection. To isolate NMDAR-mediated EPSCs in the MK-801 experiments, $CaCl_2$ and $MgCl_2$ were lowered to 1.5 and 0.1 mM, respectively, and aCSF was supplemented with an NMDAR co-agonist (20 μM glycine) and an AMPAR blocker (2 μM NBQX). The intracellular solution contained (in mM): 100 K-gluconate, 5 K-glutamate, 17 KCl, 5 NaCl, 0.5 EGTA, 5 $MgCl_2$, 4 K_2-ATP, 0.5 Na_3-GTP, 20 K_2-creatine phosphate, 10 HEPES-KOH (pH 7.28; osmolarity adjusted to 280 mOsm). Recordings were performed with two Axopatch 200B amplifiers (Molecular Devices). Pipette resistances were 2-3 MΩ; series resistances were always below 20 MΩ, stable (<20% variation), not significantly different between conditions, and compensated by 70% in the postsynaptic cell. Pre- and postsynaptic neurons were voltage-clamped at -70 and -50 mV for AMPAR- and NMDAR-mediated EPSC recordings, respectively; in order to evoke synaptic transmission, unclamped Na^+ spikes were elicited in the presynaptic neuron by delivering one or two depolarizing stimuli (+30 mV, 2 ms-long) at various interstimulus

intervals. Signals were filtered at 2 kHz, digitized at 20 kHz using Clampex 10.1 (Molecular Devices) and analyzed offline with Clampfit 10.1 (Molecular Devices) and Igor Pro 6.03 (Wavemetrics Inc.). Paired-pulse stimulations were delivered every 20 s; each paired-pulse series (10, 25, 50, 100, and 200 ms paired-pulse intervals) was repeated at least three times and averaged for each cell before calculating PPR (Kim and Alger, 2001). NMDAR-mediated EPSCs were evoked every 10 s; after a stable baseline was obtained (≥12 stimuli), stimulation was stopped, neurons were voltage-clamped at −70 mV and MK-801 (5 μM) was perfused for 3 min before resuming stimulation (100 stimuli) in the continuous presence of MK-801.

For overlapping EPSC pairs, the peak amplitude of the second EPSC was estimated as follows: all non-overlapping EPSCs from the same cell were averaged, the resulting mean EPSC was synchronized with and scaled to the peak of the first EPSC in the overlapping pair, and subtracted from the second EPSC; the resulting peak was taken as best amplitude estimation of the second EPSC.

To measure the coefficient of variation (CV) of the first EPSC, synaptic responses were base-lined using a 10 ms window immediately preceding the start of the EPSCs, and then averaged. A measurement window of 1 ms was placed at the peak of the averaged EPSC to measure synaptic responses. To measure the background noise, a second measurement window of 1 ms preceded the baseline in such a way that the baseline window was equidistant between the two measurement windows. CV was then calculated as $CV=\sqrt{(\sigma^2_p-\sigma^2_b)}/\mu_p$ where μ_p is the mean of the EPSC peak, σ^2_p the variance of the EPSC peak and σ^2_b the variance of the background noise (Cingolani and Goda, 2008; Silver, 2003).

Synaptic latency, measured from the end of the presynaptic Na^+ spike to 5% of the EPSC amplitude (Boudkkazi et al., 2007), was not modified by EF-hand-like splice isoforms (EFa pre: 2.45 ± 0.54 ms; EFa post: 2.57 ± 0.67 ms; EFb pre: 2.84 ± 0.33 ms; EFb post: 2.49 ± 0.70 ms; p = 0.95). Similarly, input resistance (R_{in}), membrane capacitance (C_m) and resting membrane potential (V_m) were not significantly affected by expression of $Ca_v2.1$[EFa] or $Ca_v2.1$[EFb] (R_{in} (in MΩ): 499 ± 38; 495 ± 25; 413 ± 20; p = 0.39; C_m (in pF): 219 ± 9; 200 ± 10; 229 ± 8; p = 0.49; V_m (in mV): -63.9 ± 1.4; -64.2 ± 1.2; -63.6 ± 0.8; p = 0.97; n = 14, 17 and 31 for EFa, EFb and Control, respectively).

Electrophysiology and optogenetics in acute brain slices

All experiments were performed in accordance with EU and Italian regulations. Fifteen-24 days post-injection, male Sprague Dawley rats were decapitated under deep isoflurane anesthesia and sagittal slices of the hippocampal formation (350 μm thick) were prepared with a Vibratome (Leica VT1200S) under low-light conditions. Slices were maintained submerged in gassed (95% O_2, 5% CO_2) aCSF containing (in mM): 123 NaCl, 1.25 KCl, 1.25 KH_2PO4, 1.5 $MgCl_2$, 1 $CaCl_2$, 25 $NaHCO_3$, 2 NaPyruvate and 18 glucose (osmolarity adjusted to 300 mOsm). After recovering for 30 min at 37°C and for ≥30 min at room temperature, slices were transferred to a submerged recording chamber and superfused at 2 ml/min with the same aCSF used for recovery supplemented with 1.5 mM $CaCl_2$ (total Ca^{2+}: 2.5 mM). Tight-seal whole-cell recordings were obtained from pyramidal neurons in the proximal to medial tract of the CA1 region under visual control using infrared illumination. Patch electrodes (5-6 MΩ) were filled with an intracellular solution containing (in mM): 110 K-gluconate, 22 KCl, 5 NaCl, 0.5 EGTA, 3 $MgCl_2$, 4 Mg-ATP, 0.5 Na_3-GTP, 20 K_2-creatine phosphate, 10 HEPES-KOH (pH 7.28; osmolarity adjusted to 290 mOsm). Experiments were performed in the presence of 10 μM Bicuculline, to block inhibitory synaptic transmission, and started after ~10 min following breakthrough. EPSCs were evoked with a 473 nm Blue Laser (MBL-III-473 Solid State 1-200mW; Information Unlimited) coupled via a 20x 0.40 N.A. objective to an optical fiber (250 μm in diameter) positioned directly on CA3 somata. Care was taken to shine light away from the Schaffer collaterals, so to avoid direct depolarization of the axons. Whenever applied (in 20 out of 39 recordings), TTX always completely blocked EPSCs (**figure S5B, C**), showing that optically evoked EPSCs are AP-driven. Stimulation length was set to 2 ms and inter-pulse to 50 ms because the ultrafast channelrhodopsin ChETA responds most reliably at these stimulations without displaying extra-spikes (Gunaydin et al., 2010). Stimulation strength (1–3 mW at fiber exit) was adjusted with neutral density filters to yield small, but clearly detectable, EPSCs (<30 pA peak amplitude at −70 mV; **figure 6D, S5D, E**). Using these conditions, optical stimulation every 20 sec reliably produced stable EPSCs for the time of the experiment (37 minutes; **figure S5B**). To prevent unspecific binding on glass and plastic surfaces, ω-conotoxin-GVIA (1 μM) was applied in the presence of cytochrome C (30 μg/ml). Nineteen out of 39 experiments were terminated with NBQX application (10 μM), which always completely blocked EPSCs (**figure S5B, C**), showing that optically-evoked EPSCs are mediated by AMPARs. Data were low-pass filtered at 5 kHz and acquired at 50 kHz with EPC10 amplifier (HEKA) and PatchMaster software (HEKA). Analysis was performed offline using Clampfit 10.1 (Molecular Devices) and Igor Pro 6.03 (Wavemetrics Inc.). Series resistances were always ≤25 MΩ, not significantly different between experimental groups, and left uncompensated. Cells were rejected if series resistance changed by more than 20% during the course of the experiment. Twenty-four traces during baseline and the last 24 traces during ω-conotoxin-GVIA application were averaged before calculating PPR (Kim and Alger, 2001).

Synaptic latency, measured from the end of the light pulse to 5% of the EPSC amplitude (Boudkkazi et al., 2007), was not modified by $Ca_v2.1$[EFa] or $Ca_v2.1$[EFb] knockdown (miR Control: 6.67 ± 0.25 ms; miR EFa1: 6.71 ± 0.25 ms; miR EFa3: 6.71 ± 0.18 ms; miR EFb2: 6.59 ± 0.17 ms; p = 0.99). Similarly, input resistance (R_{in}), membrane capacitance (C_m) and resting membrane potential (V_m) were not significantly different between experimental conditions (R_{in} (in MΩ): 204 ± 11; 184 ± 6; 202 ± 4; 178 ± 4; p = 0.53; C_m (in pF): 501 ± 21; 449 ± 23; 512 ± 16;

424 ± 20; p = 0.36; V_m (in mV): -60.2 ± 0.6; -58.8 ± 0.7; -57.9 ± 0.6; -60.6 ± 0.7; p = 0.37; n = 12, 9, 9 and 11 for miR Control, miR EFa1, miR EFa3 and miR EFb2, respectively).

Presynaptic Ca^{2+} imaging with SyGCaMP3 and SyGCaMP6s

Imaging was performed in rat primary cultures at room temperature in aCSF containing (in mM): 140 NaCl, 2.5 KCl, 2.2 $CaCl_2$, 1.5 $MgCl_2$, 10 D-glucose, 0.01 CNQX, 0.05 D-APV and 10 HEPES-NaOH (pH 7.38; osmolarity adjusted to 290 mOsm). For experiments in **figure S3A-C**, we selected SyGCaMP3 (K_D=345-405 nM; Hill coefficient = 2.10-2.54 for GCaMP3) (Akerboom et al., 2012; Chen et al., 2013) as Ca^{2+} reporter because it displayed the lowest cooperative behavior amongst the Ca^{2+} indicators we tested (GCaMP3, GCaMP5g and GCaMP6s). Cultures were co-transfected with SyGCaMP3, the auxiliary subunit β4 and $Ca_v2.1$[EFa] or $Ca_v2.1$[EFb] in a 1:1:1 DNA ratio 3-5 days prior to experiments, and measured at 13-15 DIV.

For experiments in **figure S4D-F**, we selected SyGCaMP6s (K_D=144 nM; Hill coefficient = 2.90 for GCaMP6s) (Chen et al., 2013) as Ca^{2+} reporter because, despite its highly non-linear behavior, it was the most sensitive amongst the Ca^{2+} indicators we tested, enabling us to detect presynaptic Ca^{2+} transients also after partial blockade of Ca^{2+} entry. Cultures were co-transfected with SyGCaMP6s and the required miR construct in a 1:1 DNA ratio 6-8 days prior to experiments, and measured at 16-18 DIV. Experiments were performed in the presence of ω-conotoxin GVIA (1 µM) to block N-type Ca^{2+} channels. Because P/Q-type and N-type Ca^{2+} channels give the largest contribution to synaptic transmission at hippocampal synapses (Reid et al., 1998; Scholz and Miller, 1995), this experimental configuration enabled us to investigate the contribution of P/Q-type channel splice isoforms to presynaptic Ca^{2+} in relative isolation.

Boutons were imaged using a cooled charge-coupled device (CCD) camera (ORCA-R2, Hamamatsu) mounted on an inverted microscope (DMI6000B, Leica) with a 40x, 1.25 NA oil immersion objective. A 200W metal halide lamp (Lumen200Pro, Prior Scientific) and a filter set comprising a BP 470/40 nm excitation filter, a 500 nm dichroic mirror and a BP 525/50 emission filter (Leica) were used for illumination. Images were captured at 15.3 Hz with 50 ms integration times at a depth of 8 bits. APs were evoked by field stimulation (60 V, 1 ms pulses; Isolated Pulse Stimulator, A-M systems) using a custom-made chamber with two parallel platinum wires 6 mm apart. Trains of APs were delivered at a frequency of 40 Hz every 18 s.

Images were analyzed in ImageJ (http://rsb.info.nih.gov/ij) with the plugin Time Series Analyzer V2.0 (http://rsb.info.nih.gov/ij/plugins/time-series.html) and with customized routines in Igor Pro 6.03. Regions of interest (ROIs) with a diameter of 3.2 µm were positioned on all boutons responding to six APs for SyGCaMP3 and to 20 APs for SyGCaMP6s with a signal above two SD of the background noise. The intensity of a twin ROI positioned within 10 µm from the first was used to subtract the local background noise. Signals were quantified as $\Delta F/F_0$, where $\Delta F=F-F_0$, with F_0 measured over 1 s period prior to stimulation.

Presynaptic Ca^{2+} imaging with Fluo-4

Imaging was performed at room temperature in aCSF containing (in mM): 125 NaCl, 2.5 KCl, 1 $CaCl_2$, 3 $MgCl_2$, 20 D-glucose, 0.01 CNQX, 0.05 D-APV and 25 HEPES-NaOH (pH 7.40; osmolarity adjusted to 310 mOsm) as previously described (Ermolyuk et al., 2012). Briefly, neurons were loaded via a whole-cell patch pipette with a mixture of the high affinity Ca^{2+} fluorescence dye Fluo-4 (200 µM, Invitrogen) and the morphological tracer Alexa 568 (200 µM, Invitrogen), added to an intracellular solution containing (in mM) 135 K-methanesulfonate, 10 HEPES, 10 Na-Phosphocreatine, 4 $MgCl_2$, 4 Na_2-ATP, 0.4 Na_3-GTP. Five minutes after breaking in, the patch pipette was slowly withdrawn to minimize cytosol dialysis. Ca^{2+} fluorescence recordings were started at least 30 min after retracting the patch pipette to allow the fluorophores to equilibrate throughout the neuron. APs were evoked by field stimulation via platinum bath electrodes separated by 1 cm (12.5 – 15 V, 1 ms pulses). Fluorescence transients in identified boutons were recorded in response to alternating single and double pulse (at 40 Hz) stimulation in fast line-scan mode (~ 500 Hz, 5 trials averaged for analysis) using an inverted LSM 510 confocal microscope (Zeiss) equipped with a 63x (1.4 NA) oil immersion objective. To minimize optical artifacts, the Fluo-4 fluorescence was normalized to the average Alexa 568 fluorescence determined in each sweep (G(t)/R ratio). The amplitude of the Ca^{2+} influx during the first AP ($\Delta G_1/R$) was calculated by subtracting the resting fluorescence (G_{rest}/R) from the fluorescence signal integrated over a 10 ms window immediately after the first AP (G_{AP}/R). The amplitude of the Ca^{2+} influx during the second AP ($\Delta G_2/R$) was calculated in a similar manner, after subtracting the Ca^{2+} fluorescence to a single AP from the Ca^{2+} fluorescence to a pair of APs (**figure S3F**).

Fluo-4 provides a linear readout of AP-evoked presynaptic Ca^{2+} influx if the $\Delta G/G_{max}$ ratio is below 0.6 (where G_{max} is the maximal fluorescence of the saturated Fluo-4 signal determined with 100 APs delivered at 100 Hz (Ermolyuk et al., 2012)). To meet this requirement, we determined that the ratio G_{max}/R was always below two in our experimental conditions, and excluded from the analysis all the boutons where the response to the first AP ($\Delta G_1/R$) was higher than 0.6 (this corresponding to a cutout of $\Delta G/G_{max} \leq 0.3$ for a single AP). We also excluded from the analysis all boutons where $\Delta G_1/R$ was lower than 0.1 because a poor signal to noise ratio in these boutons precluded us from reliably determining $\Delta G_2/\Delta G_1$.

Imaging of vesicle cycling with synaptophysin-pHluorin

Synaptophysin-pHluorin (SypHy) was imaged in aCSF containing (in mM): 140 NaCl, 2.5 KCl, 2.2 $CaCl_2$, 1.5

$MgCl_2$, 13 D-glucose, 0.01 CNQX, 0.05 D-APV and 12 HEPES-NaOH (pH 7.38; osmolarity adjusted to 320 mOsm). Alkalization of the entire vesicle pool was achieved with aCSF differing from the above for the presence of NH_4Cl (50 mM) and for a reduced content of NaCl (60 mM). For experiments in **figure 3A, B**, cultures were co-transfected with SypHy, the auxiliary subunit β4 and $Ca_v2.1$[EFa] or $Ca_v2.1$[EFb] in a 1:1:1 DNA ratio 3-4 days prior to experiments, and measured at 13-14 DIV. For experiments in **figure 5**, cultures were co-transfected with SypHy and the required miR construct in a 1:1 DNA ratio 6-8 days prior to experiments, and measured at 16-18 DIV. Under basal conditions, SypHy responses in the knockdown experiments were considerable larger than those in the over-expression experiments (compare figure 5B with 3B). This is because of differences in culture age, time of expression and amount of SypHy DNA used for transfection in the two sets of experiments (A.T. and L.A.C., unpublished observations). SypHy responses were stable and reproducible for the time period of the experiment (16 min). EGTA-AM (200 μM) was loaded for 90 s, followed by 10 min wash (Hoppa et al., 2012). In control experiments, application of DMSO at the same final concentration used to dissolve EGTA-AM (0.1%) did not affect SypHy responses (n=3, 3 and 2 independent experiments for $Ca_v2.1$[EFa], $Ca_v2.1$[EFb] and Control, respectively). Images were captured at 2 Hz with 100 ms integration times and analyzed offline in ImageJ as for SyGCaMP experiments. Signals were background subtracted and quantified as $\Delta F=F-F_0$, where F_0 was measured over a 5 s period prior to stimulation.

Synaptotagmin antibody live uptake and confocal microscopy

Imaging was performed as previously described (Cingolani et al., 2008). Briefly, primary hippocampal cultures were transfected at 10 DIV and fixed at 14 and 17-18 DIV for the over-expression and knockdown experiments, respectively. Fixation was performed with 4% paraformaldehyde/4% sucrose (12 min), permeabilization with methanol (-20°C; 10 min on ice) followed by 0.2% Triton X-100 (10 min) (Liao et al., 1999) and blocking with 4% NGS/0.1% BSA (30 min). The following primary antibodies were used: chicken anti-GFP (1:1000; Cat. No. 13970, Abcam), rabbit anti-$Ca_v2.1$ (1:1000; Cat. No. 152203, Synaptic Systems), rabbit anti-$Ca_v2.1$ (1: 250; Cat. No. 152103, Synaptic Systems; this antibody was used for experiments in figure S2A-B, as it is specific for rodent $Ca_v2.1$ (Schneider et al., 2015), rabbit anti $Ca_v2.2$ (1:100; Cat. No. ACC-002, Alomone Labs), mouse anti-RFP (1:2000; Cat. No. 200-301-379, tebu-bio) and guinea pig anti-bassoon (1:500; Cat. No. 141004, Synaptic Systems). Secondary antibodies were Alexa488 goat anti-chicken, Alexa488 goat anti-rabbit, Alexa568 goat anti-rabbit, Alexa568 goat anti-mouse and Alexa647 goat anti-guinea pig IgGs (1:1000 in all cases; Cat. No. A11039, A11034, A11036, A11031 and A21450, respectively, Invitrogen). Confocal stacks were acquired at 200 Hz with a Leica SP8 using a 63x oil immersion objective (NA 1.40), 1.2x digital zoom, 0.15 μm pixel size, 1 AU pinhole, 0.3 μm between optical sections, with a sequential line-scan mode and 3x scan averaging. For all experimental conditions compared, the same settings for laser intensity, offset and PMT gain were used.

Confocal images were analyzed using ImageJ. Each single stack was filtered using a Gaussian filter (radius: 0.5 pixels), and the maximal fluorescence intensities of in-focus stacks were Z-projected. Analysis of fluorescence intensity was performed on axonal ROIs (2-3 per image) of 50-150 μm in lengths, manually selected blind to the experimental condition. The ROIs were automatically thresholded using a fixed value (30 a.u.) for $Ca_v2.1$ over-expressed constructs, mode plus three standard deviations of the gray scale histogram for endogenous $Ca_v2.1$, mode plus half standard deviation of the gray scale histogram for TdTomato and the Robust Automatic Threshold Selection plugin for bassoon. Colocalization between bassoon and $Ca_v2.1$ was estimated for the thresholded ROIs with the Coloc2 plugin using the Manders' coefficients ($M_A=\sum_i A_{i,coloc}/\sum_i A_i$, where $\sum_i A_i$ is the sum of intensities of all pixels above threshold for channel A and $\sum_i A_{i,coloc}$ is calculated as $\sum_i A_i$ but only for pixels where also the second channel B is above threshold).

For the synaptotagmin antibody live uptake, we treated cultures with CNQX (20 μM) and D-APV (100 μM) 24 hours prior to experiment. This protocol is very effective in inducing presynaptic homeostatic plasticity, including up-scaling of presynaptic P/Q-type channels (Lazarevic et al., 2011), while differentially affecting $Ca_v2.1$ splice isoform expression at the mRNA level (**figure 7A**). We blocked N-type Ca^{2+} channels with ω-conotoxin GVIA (1 μM) starting 30 min prior to uptake in order to investigate the contribution of P/Q-type channel splice isoforms to vesicle release in relative isolation (Reid et al., 1998; Scholz and Miller, 1995). A subset of coverslips treated also with ω-agatoxin TK (300 nM) for the same time period served as negative control. Neurons were rinsed twice in aCSF containing (in mM): 140 NaCl, 5 KCl, 2.2 $CaCl_2$, 1.5 $MgCl_2$, 15 D-glucose, 0.01 CNQX, 0.05 D-APV, 0.001 ω-conotoxin GVIA and 12 HEPES-NaOH, with or without 0.0003 ω-agatoxin TK (pH 7.38; osmolarity adjusted to 320 mOsm), before performing the synaptotagmin antibody live uptake in the same aCSF for 12 min at 37°C with a mouse antibody against the luminal domain of synaptotagmin 1 (1:200; Cat. No. 105311, Synaptic Systems). In initial cell-attached and whole-cell electrophysiological recordings, we established that these conditions support spontaneous neuronal firing at low rate (≤10 Hz), thus being suitable for detecting activity-dependent changes in presynaptic activity (Lazarevic et al., 2011). After three washes in the same aCSF, neurons were fixed and processed for immunofluorescence as above. The following primary antibodies were used: chicken anti-RFP (1:500; Cat. No. 600-901-379, tebu-bio) and rabbit anti-$Ca_v2.1$ (1:1000; Cat. No. 152203, Synaptic Systems). Secondary antibodies were Alexa488-, Alexa568- and Alexa647-conjugated goat anti-mouse, anti-chicken and anti-rabbit (1:1000 in all cases; Cat. No. A11029, A11041 and A21245, respectively, Invitrogen).

Confocal images were acquired and analyzed as above with the following modifications: active boutons within

TdTomato-positive axons were selected blind to the experimental conditions in the synaptotagmin channel using the ImageJ plugin Time Series Analyzer V3.0 (circular ROIs, Ø 1.2 µm). The synaptotagmin and $Ca_v2.1$ signals within each ROI were then automatically thresholded using a fixed value (22 a.u.) for all conditions.

Statistical analysis

Unless otherwise stated, statistical differences were assessed using paired and unpaired two-tailed Student's t-test, and the one-way analysis of variance test followed by the Tukey-Kramer post-test, as required. The analysis of covariance was used for figures 1E, 3D, 6E and S5F; the Kruskal-Wallis test followed by the Dunn's multiple comparison post-test for figure 1G; the one-way analysis of variance test followed by the linear trend post-test to analyze the correlation between synaptotagmin uptake and $Ca_v2.1$ signal in figure S6B (Prism 5, GraphPad Software Inc.); the Kolmogorov-Smirnov test for figure S4F (http://www.physics.csbsju.edu/stats/KS-test.n.plot_form.html). Unless otherwise stated, average data are expressed as mean+SEM.

Supplemental references

Akerboom, J., Chen, T.W., Wardill, T.J., Tian, L., Marvin, J.S., Mutlu, S., Calderon, N.C., Esposti, F., Borghuis, B.G., Sun, X.R.*, et al.* (2012). Optimization of a GCaMP calcium indicator for neural activity imaging. J Neurosci *32*, 13819-13840.

Boudkkazi, S., Carlier, E., Ankri, N., Caillard, O., Giraud, P., Fronzaroli-Molinieres, L., and Debanne, D. (2007). Release-dependent variations in synaptic latency: a putative code for short- and long-term synaptic dynamics. Neuron *56*, 1048-1060.

Bourinet, E., Soong, T.W., Sutton, K., Slaymaker, S., Mathews, E., Monteil, A., Zamponi, G.W., Nargeot, J., and Snutch, T.P. (1999). Splicing of alpha 1A subunit gene generates phenotypic variants of P- and Q-type calcium channels. Nat Neurosci *2*, 407-415.

Cao, Y.Q., Piedras-Renteria, E.S., Smith, G.B., Chen, G., Harata, N.C., and Tsien, R.W. (2004). Presynaptic Ca2+ channels compete for channel type-preferring slots in altered neurotransmission arising from Ca2+ channelopathy. Neuron *43*, 387-400.

Cao, Y.Q., and Tsien, R.W. (2010). Different relationship of N- and P/Q-type Ca2+ channels to channel-interacting slots in controlling neurotransmission at cultured hippocampal synapses. J Neurosci *30*, 4536-4546.

Chaudhuri, D., Chang, S.Y., DeMaria, C.D., Alvania, R.S., Soong, T.W., and Yue, D.T. (2004). Alternative splicing as a molecular switch for Ca2+/calmodulin-dependent facilitation of P/Q-type Ca2+ channels. J Neurosci *24*, 6334-6342.

Chen, T.W., Wardill, T.J., Sun, Y., Pulver, S.R., Renninger, S.L., Baohan, A., Schreiter, E.R., Kerr, R.A., Orger, M.B., Jayaraman, V.*, et al.* (2013). Ultrasensitive fluorescent proteins for imaging neuronal activity. Nature *499*, 295-300.

Cingolani, L.A., and Goda, Y. (2008). Differential involvement of beta3 integrin in pre- and postsynaptic forms of adaptation to chronic activity deprivation. Neuron Glia Biol *4*, 179-187.

Cingolani, L.A., Thalhammer, A., Yu, L.M., Catalano, M., Ramos, T., Colicos, M.A., and Goda, Y. (2008). Activity-dependent regulation of synaptic AMPA receptor composition and abundance by beta3 integrins. Neuron *58*, 749-762.

Deidda, G., Parrini, M., Naskar, S., Bozarth, I.F., Contestabile, A., and Cancedda, L. (2015). Reversing excitatory GABAAR signaling restores synaptic plasticity and memory in a mouse model of Down syndrome. Nat Med *21*, 318-326.

Dreosti, E., Odermatt, B., Dorostkar, M.M., and Lagnado, L. (2009). A genetically encoded reporter of synaptic activity in vivo. Nat Methods *6*, 883-889.

Ermolyuk, Y.S., Alder, F.G., Henneberger, C., Rusakov, D.A., Kullmann, D.M., and Volynski, K.E. (2012). Independent regulation of Basal neurotransmitter release efficacy by variable Ca(2)+ influx and bouton size at small central synapses. PLoS Biol *10*, e1001396.

Gunaydin, L.A., Yizhar, O., Berndt, A., Sohal, V.S., Deisseroth, K., and Hegemann, P. (2010). Ultrafast optogenetic control. Nat Neurosci *13*, 387-392.

Hoppa, M.B., Lana, B., Margas, W., Dolphin, A.C., and Ryan, T.A. (2012). alpha2delta expression sets presynaptic calcium channel abundance and release probability. Nature *486*, 122-125.

Kim, J., and Alger, B.E. (2001). Random response fluctuations lead to spurious paired-pulse facilitation. J Neurosci *21*, 9608-9618.

Lazarevic, V., Schone, C., Heine, M., Gundelfinger, E.D., and Fejtova, A. (2011). Extensive remodeling of the presynaptic cytomatrix upon homeostatic adaptation to network activity silencing. J Neurosci *31*, 10189-10200.

Li, H., Foss, S.M., Dobryy, Y.L., Park, C.K., Hires, S.A., Shaner, N.C., Tsien, R.Y., Osborne, L.C., and Voglmaier, S.M. (2011). Concurrent imaging of synaptic vesicle recycling and calcium dynamics. Front Mol Neurosci *4*, 34.

Liao, D., Zhang, X., O'Brien, R., Ehlers, M.D., and Huganir, R.L. (1999). Regulation of morphological postsynaptic silent synapses in developing hippocampal neurons. Nat Neurosci *2*, 37-43.

McClure, C., Cole, K.L., Wulff, P., Klugmann, M., and Murray, A.J. (2011). Production and titering of recombinant adeno-associated viral vectors. J Vis Exp, e3348.

Niwa, H., Yamamura, K., and Miyazaki, J. (1991). Efficient selection for high-expression transfectants with a novel eukaryotic vector. Gene *108*, 193-199.

Qian, J., and Noebels, J.L. (2000). Presynaptic Ca(2+) influx at a mouse central synapse with Ca(2+) channel subunit mutations. J Neurosci *20*, 163-170.

Reid, C.A., Bekkers, J.M., and Clements, J.D. (1998). N- and P/Q-type Ca2+ channels mediate transmitter release with a similar cooperativity at rat hippocampal autapses. J Neurosci *18*, 2849-2855.

Saunders, A., Johnson, C.A., and Sabatini, B.L. (2012). Novel recombinant adeno-associated viruses for Cre activated and inactivated transgene expression in neurons. Front Neural Circuits *6*, 47.

Scheuber, A., Miles, R., and Poncer, J.C. (2004). Presynaptic Cav2.1 and Cav2.2 differentially influence release dynamics at hippocampal excitatory synapses. J Neurosci *24*, 10402-10409.

Schneider, R., Hosy, E., Kohl, J., Klueva, J., Choquet, D., Thomas, U., Voigt, A., and Heine, M. (2015). Mobility of calcium channels in the presynaptic membrane. Neuron *86*, 672-679.

Scholz, K.P., and Miller, R.J. (1995). Developmental changes in presynaptic calcium channels coupled to glutamate release in cultured rat hippocampal neurons. J Neurosci *15*, 4612-4617.

Silver, R.A. (2003). Estimation of nonuniform quantal parameters with multiple-probability fluctuation analysis: theory, application and limitations. J Neurosci Methods *130*, 127-141.

Thalhammer, A., and Cingolani, L.A. (2014). Cell adhesion and homeostatic synaptic plasticity. Neuropharmacology *78*, 23-30.

Vandesompele, J., De Preter, K., Pattyn, F., Poppe, B., Van Roy, N., De Paepe, A., and Speleman, F. (2002). Accurate normalization of real-time quantitative RT-PCR data by geometric averaging of multiple internal control genes. Genome Biol *3*, RESEARCH0034.

Wu, L.G., and Saggau, P. (1994). Pharmacological identification of two types of presynaptic voltage-dependent calcium channels at CA3-CA1 synapses of the hippocampus. J Neurosci *14*, 5613-5622.